

17 **Abstract**

18 Volcanic eruptions have a significant impact on climate when they inject sulfur gases into
19 the stratosphere. The dynamics of eruption plumes is also affected by climate itself, as
20 atmospheric stratification impacts plumes height. We use an integral plume model to
21 assess changes in volcanic plume maximum rise heights as a consequence of global warm-
22 ing, with atmospheric conditions from an ensemble of global climate models (GCM), us-
23 ing three representative concentration pathways (RCP) scenarios. Predicted changes in
24 atmospheric temperature profiles decrease the heights of tropospheric and lowermost strato-
25 spheric volcanic plumes and increase the tropopause height, for the RCP4.5 and RCP8.5
26 scenarios in the coming three centuries. Consequently, the critical mass eruption rate
27 required to cross the tropopause increases by up to a factor 3 for tropical regions, and
28 up to 2 for high-latitude regions. A number of recent lower stratospheric plumes, mostly
29 in the tropics (e.g., Merapi, 2010), would be expected to not cross the tropopause start-
30 ing from the late 21st century, under RCP4.5 and RCP8.5 scenario. This effect could re-
31 sult in a $\simeq 5 - 25\%$ decrease in the average SO₂ flux into the stratosphere carried by
32 small plumes, which frequency is larger than the rate of decay of volcanic stratospheric
33 aerosol, and a $\simeq 2 - 12\%$ decrease of the total flux. Our results suggest the existence
34 of a positive feedback between climate and volcanic aerosol forcing. Such feedback may
35 have minor implications for global warming rate but can prove to be important to un-
36 derstand the long-term evolution of volcanic atmospheric inputs.

1 Introduction

Explosive volcanic eruptions eject gases and ash into the atmosphere, which act to modify Earth's global radiative energy balance. At annual to centennial timescales, the injection of sulfur gases, resulting in the formation of sulfur aerosols, has the largest impact on Earth's radiative balance via scattering of Sun radiation and absorption of Sun and Earth radiation (aerosol-radiation interactions) [Robock, 2000; Timmreck, 2012]. Tropospheric volcanic aerosols are washed out within a few weeks. It is therefore commonly assumed that tropospheric aerosol-radiation interactions from individual eruptions are negligible at a global scale, although aerosol particles enhance cloud condensation nuclei and, thus, have an indirect impact via aerosol-cloud interactions on Earth's radiative balance [Schmidt *et al.*, 2012]. Stratospheric volcanic aerosols, by comparison, have a typical e-folding time of one year and exert a significant influence on climate over these timescales. These relatively long-lived particles scatter shortwave radiation and absorb longwave radiation, resulting in a net cooling of the troposphere and a net warming of the stratosphere [Robock, 2000; Timmreck, 2012]. In addition to these global effects on air temperature, stratospheric volcanic aerosol-radiation interactions can cause significant changes in atmospheric and oceanic circulation, sea ice dynamics (e.g., Robock [2000]; Shindell *et al.* [2004]; Mignot *et al.* [2011]; McGregor and Timmermann [2010]; Driscoll *et al.* [2012]; Stoffel *et al.* [2015]; Toohey *et al.* [2016a]), and precipitation patterns (e.g., Iles and Hegerl [2015]). Whether an eruptive plume reaches the stratosphere also controls ozone depletion by halogen species injected by a volcano, although this forcing is small relative to aerosol-radiation interactions and largely depends on halogen scavenging in the plume [Tabazadeh and Turco, 1993; Textor *et al.*, 2003; Timmreck, 2012; Carn *et al.*, 2016].

In the context of present day global warming, which is mostly driven by anthropogenic greenhouse gas emissions, volcanic aerosols are of particular importance because their atmospheric temperature fingerprint is opposed to the one of CO₂, i.e., a net warming of the troposphere and a net cooling of the stratosphere [Hartmann *et al.*, 2013]. In particular, climate models neglecting aerosol-radiation interactions of stratospheric volcanic eruptions since 1998 are overestimating global warming, even though no major volcanic eruption occurred during this period [Solomon *et al.*, 2011; Haywood *et al.*, 2014; Ridley *et al.*, 2014; Santer *et al.*, 2014].

69 Critically, most projections from global climate models (GCMs) impose a constant
 70 volcanic radiative forcing [*Collins et al.*, 2013a]. Only some decadal projections exper-
 71 iments assume that a Pinatubo-like eruption will occur at one given year to test sensi-
 72 tivity of short-term projections to volcanic eruptions [*Taylor et al.*, 2012]. Thus, GCMs
 73 are unable to predict temperature changes resulting from future eruptions, although their
 74 ability to simulate the climate response to past volcanic eruptions is continuously im-
 75 proved [*Timmreck*, 2012; *Flato et al.*, 2013]. Prediction of changes in future volcanic aerosol-
 76 radiation interaction would allow improved prediction of future climate.

77 There are two key controls on volcanic aerosol-radiation interactions resulting from
 78 a particular eruption:

- 79 1. How much sulfur gas is expelled.
- 80 2. Whether this sulfur gas reaches the stratosphere.

81 Both controls partly depend on eruption source conditions, and, in particular, on
 82 the mass eruption rate of the eruptive plume. The exact timing, global location, and source
 83 conditions of future eruptions are impossible to predict, which is a reason why most cli-
 84 mate projections assume a constant volcanic radiative forcing. In addition, the height
 85 of a given volcanic plume H depends strongly on atmospheric stratification [*Morton et al.*,
 86 1956; *Wilson et al.*, 1978; *Woods*, 2010]:

$$87 \quad H \propto N^{-\kappa_1} M_0^{\kappa_2} , \quad (1)$$

88 where N is the Brunt-Väisälä frequency, M_0 is the mass eruption rate, $\kappa_1 = \frac{3}{4}$ and $\kappa_2 = \frac{1}{4}$
 89 in the absence of wind [*Morton et al.*, 1956] and $\kappa_1 = \frac{2}{3}$ and $\kappa_2 = \frac{1}{3}$ under strong wind con-
 90 ditions [*Hewett et al.*, 1971]. The Brunt-Väisälä frequency mostly depends on the tem-
 91 perature lapse rate :

$$92 \quad N^2 = \frac{g}{T} \left(\frac{g}{c_p} - \Gamma \right) , \quad (2)$$

93 where g is the Earth's gravitational acceleration, T is the atmospheric temperature, c_p
 94 is the air specific heat capacity, $\Gamma = -\frac{dT}{dz}$ is the lapse rate and z is the altitude.

95 A major effect of present day global warming is the decrease of the temperature
 96 lapse rate Γ in the tropical troposphere (e.g., *Simmons et al.* [2014]; *Sherwood and Nis-*

97 *hant* [2015]), and hence an increase in the strength of the stratification which could re-
98 sult in a decrease of tropospheric plume height, in the tropics (Equation 1). The key ques-
99 tion we ask in this paper is, thus: how will global warming impact the heights of plumes
100 of future eruptions? In particular, will more or fewer eruptive plumes reach the strato-
101 sphere than at present, and how will it impact future volcanic aerosol-radiation inter-
102 actions? Some of these questions are raised by *Glaze et al.* [2015] in the context of past
103 climate change, but have never been investigated into detail in the context of the present
104 day climate change. Understanding the climate change-driven controls on variations in
105 volcanic plume height has fundamental implications also on the distribution of hazards
106 associated with the dispersal and sedimentation of both lapilli-sized and ash-sized par-
107 ticles, e.g., from proximal damage to buildings and infrastructures to far-field risk to avi-
108 ation and human health [*Rymer*, 2015].

109 Our paper is structured in the following way. Our methodology is described in de-
110 tail in section 2: we use an integral volcanic plume model to predict changes in volcanic
111 plume height driven by changes in atmospheric temperature, geopotential height and wind
112 fields inferred from GCM projections. In section 3, we show the impact of predicted changes
113 of these fields on the plume height, as well as the impact of their combined effects. In
114 section 4, we test the sensitivity of our results regarding the plume model parameter-
115 ization and choice of GCM. Lastly, we estimate changes in the flux of volcanic SO₂ into
116 the stratosphere driven by changes in plume height, and discuss the implications of our
117 results for future volcanic forcing.

118 **2 Data and plume model**

119 We apply an integral volcanic plume model to compute the height of explosive vol-
120 canic plumes. In each model run, we specify eruption source conditions and atmospheric
121 conditions. We use atmospheric conditions associated with 12 active volcanic regions (Fig-
122 ure 1) over four different time intervals. The sample of 12 regions is chosen based on its
123 large scatter both latitudinally and longitudinally, which facilitates the sensitivity test
124 of our results to regional climate variability. The projections for atmospheric conditions
125 are based on three different greenhouse-gas emission scenarios from an ensemble of three
126 GCMs. Our overall methodology is summarized by the flow chart presented in Figure
127 2.a and the following sections provide more details on the data and integral volcanic plume
128 model that are used.

2.1 Source conditions

Source conditions that must be specified for each run of the integral volcanic plume model are the vent altitude and radius, and the gas-ash mixture exit velocity, gas content and temperature. We use two approaches to specify the source conditions of the model. First, we sample source conditions in a fixed parameter space (Table 1). A key source parameter controlling the height reached by a volcanic plume (Equation 1) is the mass eruption rate M_0 :

$$M_0 = \pi \rho_0 R_0^2 U_0 \quad , \quad (3)$$

which is controlled by the vent radius R_0 , the exit velocity U_0 , and the bulk density of the ejected mixture ρ_0 which depends on the magma temperature and gas content. We will initially vary M_0 by considering variations in R_0 and U_0 only (section 3). The range in which we sample R_0 and U_0 is chosen to obtain mass eruption rates of $\simeq 10^6$ – 10^8 kg s $^{-1}$, which ensures that plume heights are between $\simeq 50$ – 150% of the present day tropopause height. We return to the sensitivity of our results to natural variability in other source parameters, including the vent altitude, in section 4.

Next, we use the dataset of *Carn et al.* [2016] to test the model using source conditions inferred for historical eruptions. We use this dataset because it covers a longer period and includes more eruptions than, for example, *Brühl et al.* [2015] or *Mills et al.* [2016]. The *Carn et al.* [2016] dataset includes the mass of SO $_2$, height of SO $_2$ injection, Volcanic Explosivity Index (VEI, *Newhall and Self* [1982]), vent altitude, latitude and longitude of eruptions observed by satellites since 1979. Estimates of SO $_2$ loading into the atmosphere are based on satellite measurements in the ultraviolet (UV), infrared (IR) and microwave spectral bands. We only use explosive eruptions between 1980 and 2015, of VEI larger than 3 and for which the estimated SO $_2$ injection altitude is higher than 50% of the tropopause altitude. In addition, we use three basaltic eruptions: an eruptive event at Mt Etna (2011, Italy), and the large fissure eruptions of Laki (1783-1784) and Bárðarbunga (2014-2015) in Iceland. We estimate the mass eruption rate of all historical eruptions used on the basis of the observed height reached by their plumes using the integral volcanic plume model described in Section 2.3. To do this, we specify atmospheric conditions retrieved from the National Centers for Environmental Prediction (NCEP)/National Center for Atmospheric Research (NCAR) reanalysis [*Kalnay et al.*, 1996], and all other parameters as in Table 1 except the vent altitude, and the gas con-

161 tent taken equal to 0.9 for the Bárðarbunga plume which contained little ash [*Schmidt*
162 *et al.*, 2015].

163 Table 2 summarizes the date, location, mass, altitude, and altitude range of injected
164 SO₂, and the estimated mass eruption rate of 10 explosive eruptions from the *Carn et al.*
165 [2016] dataset as well as the three basaltic eruptions used. For the Laki (1783-1784) erup-
166 tion, we use a mean plume altitude of 11 km corresponding to the range of plume alti-
167 tudes of 9-13 km estimated by *Thordarson and Self* [2003] for explosive plumes during
168 the first three months of the eruption, during which most of the SO₂ was released. Un-
169 certainties in the altitude reached by volcanic SO₂ plumes are large, including when they
170 are estimated using satellite measurements. For example, estimates from *Carn et al.* [2016]
171 are often in the higher range of values found in *Brühl et al.* [2015] or *Mills et al.* [2016].
172 Another example is the Nabro (2011) eruption, for which *Bourassa et al.* [2013] report
173 tropospheric plume altitudes of 13-16 km while *Vernier et al.* [2013] and *Fromm et al.*
174 [2013] reports stratospheric altitudes of 16-19 km.

175 Last, in Section 4, we use the ? dataset in addition to the *Carn et al.* [2016] dataset
176 to estimate SO₂ flux into the stratosphere. ? use Greenland and Antarctic ice-cores to
177 reconstruct the mass of volcanic aerosols produced in the stratosphere by eruptions over
178 the past 2500 years. Figure S3 shows the distribution of erupted mass of SO₂ using these
179 two datasets. The *Carn et al.* [2016] dataset enables to characterize small stratospheric
180 injections (≤ 3 Mt of SO₂), which occur with a frequency that is larger than the rate of
181 decay of stratospheric sulfate aerosol and contribute strongly to the “stratospheric aerosol
182 background” [*Solomon et al.*, 2011]. The ? dataset, on the other hand, enables to char-
183 acterize large stratospheric injections (≥ 3 Mt of SO₂) which occur with a frequency that
184 is much smaller than the rate of decay of stratospheric sulfate aerosol, and thus act as
185 impulsive forcings.

186 2.2 Atmospheric conditions

187 2.2.1 Choice of GCM, period and RCP scenario

188 We retrieve the temperature (T), pressure (P), horizontal wind speed (V), and rel-
189 ative humidity (RH) profiles required for each run of the integral volcanic plume model.
190 These fields are retrieved from an ensemble of three Coupled Model Intercomparison Project
191 Phase 5 (CMIP5) GCMs:

- 192 • BCC-CSM1.1 is the coarse resolution version of the Earth System Model (ESM,
193 coupled climate-carbon cycle model) of the Beijing Climate Center Climate Sys-
194 tem Model (BCC-CSM, *Wu et al.* [2014]). The horizontal resolution is approxi-
195 mately $2.8125^\circ \times 2.8125^\circ$ with 26 levels for the atmospheric component .
- 196 • CanESM2 is the Earth system model of the Canadian Centre for Climate Mod-
197 eling and Analysis [*Chylek et al.*, 2011]. The horizontal resolution is approximately
198 $1.875^\circ \times 1.875^\circ$ with 35 levels for the atmospheric component.
- 199 • MPI-ESM-LR is the Earth system model of the Max Planck Institute (MPI, *Gior-*
200 *getta et al.* [2013]). The horizontal resolution is approximately $1.875^\circ \times 1.875^\circ$ with
201 47 levels for the atmospheric component.

202 We choose these GCMs because of the availability of long-term (2005-2300) climate pro-
203 jections outputs with a daily resolution (Table S1). Profiles of fields are drawn from GCM
204 output over 8 to 15 pressure levels. Because the integral volcanic plume model uses height
205 levels and is integrated with a vertical resolution of a few tens of meters, we also retrieve
206 geopotential height (Z) profiles and interpolate the field profiles drawn from GCM re-
207 sults using a cubic interpolation scheme (after testing several interpolation methods).
208 Because the duration of large explosive eruptions is typically of the order one day (e.g.,
209 *Mastin et al.* [2009]), we use daily atmospheric variables, retrieved from 12 regions in which
210 explosive eruptions potentially reaching the stratosphere (Volcanic Explosivity Index \geq
211 3, *Newhall and Self* [1982]) most frequently occur (Figure 1, Table S2). For each region
212 we derive the spatially-averaged daily atmospheric profiles. All GCM outputs are ob-
213 tained from the Climate and Environmental Retrieval and Archive database (<http://cera->
214 www.dkrz.de/). We use [*Taylor et al.*, 2012]:

- 215 • Historical experiments where GCMs were run for the 1850-2005 period with im-
216 posed atmospheric composition (e.g., CO_2), solar forcing, aerosols, and land use
217 changes inferred from observations.
- 218 • Representative Concentration Pathways (RCP) experiments where GCMs were
219 run with different forcing scenarios, in particular in terms of CO_2 concentrations,
220 but also in terms of other greenhouse gases, aerosols and land use change. We use
221 the RCP2.6, RCP4.5 and RCP8.5 experiments, and the periods 2081-2100, 2181-
222 2200 and 2281-2300.

We take our reference period to be 1981-2000, for which data are retrieved from the historical experiments. Our choice of RCP scenarios and periods allows us to explore the impact of a large range of greenhouse gas forcings [Van Vuuren *et al.*, 2011]:

- For the RCP2.6 scenario, Earth radiative forcing peaks at $+3 \text{ W m}^{-2}$ (relative to pre-industrial period) in the mid 21st century before decreasing ($+2.6 \text{ W m}^{-2}$ in 2100, $\simeq +2 \text{ W m}^{-2}$ in 2300). In the fifth assessment report (AR5), the International Panel on Climate Change (IPCC) project global mean surface air temperature anomalies in 2081-2100 relative to 1986-2005 of 1.0 ± 0.4 , and 0.6 ± 0.3 in 2281-2300 (CMIP5 multi-model mean ± 1 standard deviation across individual models, Collins *et al.* [2013b]).
- For the RCP4.5 scenario, the radiative forcing peaks at $+4.5 \text{ W m}^{-2}$ in 2100 and is stable in the following centuries. Projected temperature anomalies for this scenario are 1.8 ± 0.5 in 2081-2100 and 2.5 ± 0.6 in 2281-2300.
- For the RCP8.5 scenario, the radiative forcing peaks at $+8.5 \text{ W m}^{-2}$ in 2100, $+12 \text{ W m}^{-2}$ in the mid 23rd century and is steady afterwards. Projected temperature anomalies for this scenario are 3.7 ± 0.7 in 2081-2100 and 7.8 ± 2.9 in 2281-2300.

Current CO₂ emissions slightly exceeded the RCP8.5 scenario over 2010-2014 [Sanford *et al.*, 2014]). For each period and RCP experiment, we use only one run for the GCMs with multiple runs available. We make this choice because for the 22nd and 23rd century, most GCMs only have outputs for the last 20 years of these centuries from a single run available (Table S1). For consistency, we used the same period duration and number of runs for the 20th and 21st centuries.

2.2.2 Performance of chosen GCMs

There is large variability in the capabilities of GCMs for reproducing past climate, as well as in their predictions of future climate. The performance of given GCMs also strongly depend on region, field variable (e.g., temperature) and altitude range [Gleckler *et al.*, 2008; Flato *et al.*, 2013]. The three GCMs (BCC-CSM1.1, CanESM2 and MPI-ESM-LR) we select for this study must perform well for all four fields (T , V , RH and Z) and in each of the 12 regions chosen. Following Gleckler *et al.* [2008], we compare how GCM historical runs reproduce climate over the 1960-2000 period, our reference period for GCM ranking. In addition to our selected three GCMs we use 13 other GCM

254 for this evaluation analysis since we are interested in the relative performance of the se-
255 lected GCMs within a model ensemble. The 16 GCMs (Table S1) are selected following
256 previous GCM evaluation studies (e.g., *Flato et al.* [2013]). We choose the NCEP-NCAR
257 reanalysis [*Kalnay et al.*, 1996] as a reference dataset, but obtain very similar results us-
258 ing the ERA40 reanalysis [*Uppala et al.*, 2005]. This section provides a brief overview
259 of our evaluation procedure and main results. The reader is referred to the Supporting
260 Information (S1) for further details.

261 GCMs are compared to the reference dataset on the basis of their root mean squared
262 errors (RMSE) assessed on (i) the monthly average of a field (T , V , RH or Z) (ii) the
263 monthly standard deviations, over time, in a field (iii) the frequency of occurrence of one
264 field characteristic profiles. For the latter metric, for a given region, month and field, we
265 demean and normalize daily profiles by subtracting the monthly mean and dividing by
266 the monthly standard deviation, at each altitude. We then identify characteristic pro-
267 files and their frequency of occurrence in the reference dataset using a Self Organizing
268 Map algorithm (SOM, *Kohonen* [1982]). Next, for each demeaned and standardized pro-
269 file of a GCM, we find the best matching profile among the characteristic profiles of the
270 reference dataset. We can then compare the frequency of occurrence of a characteristic
271 profile in a GCM and in the reference dataset [*Radić et al.*, 2015]. More details on this
272 metric are given in Supporting Information. Since we are interested in the relative model
273 performance, we define the relative RMSE as the error relative to the median error of
274 the 16 GCMs. In this way, a relative model error of, for example, 0.5 means that the GCM
275 has a 50% larger error than the median model error. Figure 3 shows the relative RMSE
276 for the three GCMs used for this study and their ensemble across all evaluation metrics.
277 For simplicity, we grouped the 12 regions into three groups of regions: northern extra-
278 tropical, tropical and southern extra-tropical region.

279 For all metrics, two of our selected GCMs (MPI-ESM-LR and Can-ESM2) perform
280 better than the median model, especially for the tropical and northern high-latitudes re-
281 gions. MPI-ESM-LR outperforms most GCMs for temperature related metrics. For BCC-
282 CSM1.1, errors are generally close to or larger than the GCM median error. The error
283 of the ensemble of the chosen three GCMs (ELT3) is always below the GCM median er-
284 ror, for errors on average fields. In particular, ELT3 outperforms most GCMs in repro-
285 ducing the mean temperature and horizontal wind speed profile (except for wind over
286 the southern extra-tropical regions). ELT3 is sometimes outperformed by CanESM2 or

287 MPI-ESM-LR. However, using this ensemble for our study will allow us to better account
 288 for uncertainties related to spread in GCMs projections of future climate. Sensitivity of
 289 our results to the choice of GCMs will be further discussed in section 4.

290 **2.3 Integral volcanic plume model**

291 To compute the height reached by a volcanic plume, we use an integral volcanic
 292 plume model described in *Degruyter and Bonadonna* [2012], which is based on the 1D
 293 buoyant plume model of *Morton et al.* [1956] adapted by *Woods* [1988] for explosive erup-
 294 tions. The model also includes the effects of atmospheric wind and humidity on the plume
 295 rise [*Bursik*, 2001; *Glaze et al.*, 1997]. We use the maximum height reached by the plume
 296 H (also called overshoot height, Figure 4), but we verified that using the height of the
 297 neutral buoyancy level H_b instead does not impact our results. Plume properties (e.g.,
 298 temperature, velocity or relative humidity) profiles across the plume are assumed to be
 299 top-hat in shape and thus depend only on the position along the plume centerline s (Fig-
 300 ure 4). Plume rise is governed by conservation equations for mass, momentum and en-
 301 ergy rates [*Degruyter and Bonadonna*, 2012].

302 Turbulent motions mix surrounding atmosphere into a rising plume. To character-
 303 ize this critical phenomenon we, employ the entrainment hypothesis [*Morton et al.*, 1956],
 304 modified to account for wind effect [*Hewett et al.*, 1971], to specify the inflow entrain-
 305 ment velocity normal to the centerline u_ϵ as:

$$306 \quad u_\epsilon = \alpha|u - V \sin(\phi)| + \beta|V \cos(\phi)| \quad . \quad (4)$$

307 Here u is the average axial velocity of the plume and ϕ is the plume deflection with re-
 308 spect to the vertical direction (Figure 4). α is the radial entrainment coefficient [*Mor-*
 309 *ton et al.*, 1956] and relates u_ϵ to the radial gradient of axial velocity. β is the wind en-
 310 trainment coefficient [*Hewett et al.*, 1971] and relates u_ϵ to the radial gradient of nor-
 311 mal velocity. The major effect of wind is to enhance entrainment rates. On the basis of
 312 the experiments of *Carazzo et al.* [2014], we take $\alpha=0.1$ and $\beta=0.7$ unless otherwise spec-
 313 ified. These values are within the range commonly used in buoyant plume models (e.g.,
 314 *Costa et al.* [2016]). Integral volcanic plume models capture the first-order effects of at-
 315 mospheric temperature and wind stresses variations on the rise of the plume (e.g., *De-*
 316 *gruyter and Bonadonna* [2012]; *Woodhouse et al.* [2013]; *Mastin* [2014]; *Folch et al.* [2016]).
 317 Uncertainties on the entrainment coefficients (Table 1) are the main sources of uncer-

318 tainty on the plume height (e.g., *Mastin* [2014], *Woodhouse et al.* [2015], *Bonadonna et al.*
319 [2015], *Costa et al.* [2016]) and will be discussed in section 4.

320 In addition to temperature and wind, atmospheric humidity can impact the plume
321 rise. Entrained water vapor can condense inside a plume, leading to an additional buoy-
322 ancy flux related to release of latent heat [*Morton*, 1957; *Woods*, 1993]. To include these
323 effects, we follow *Glaze et al.* [1997] and assume that water vapor condensation inside
324 the plume occurs at a specified constant rate λ when water vapor pressure is above the
325 saturation pressure. The reader is referred to *Degruyter and Bonadonna* [2012] for fur-
326 ther details on the integral volcanic plume model. How to most accurately capture the
327 effects of humidity on plume rise in integral models is a challenge that is largely unex-
328 plored. Furthermore, simulation of humidity and cloud formation is one of the main chal-
329 lenges for GCMs [*Flato et al.*, 2013]. Consequently, in this study, the impact of projected
330 changes in relative humidity will be discussed in section 4 but is not considered (i.e., $\lambda=0$)
331 in our main results (section 3).

332 For given eruption source conditions, region, period, and RCP scenario, the vol-
333 canic plume maximum height depends on the exact weather conditions during the erup-
334 tion. As future mean weather conditions are projected with a large range of uncertainty,
335 we apply a method that allows us to assess the probability of occurrence of most pre-
336 vailing (characteristic) weather conditions in terms of temperature, wind speed, relative
337 humidity and geopotential height. To this end, we use a SOM algorithm to cluster the
338 GCMs daily profiles from each 20-year period into $\simeq 60$ representative profiles, each of
339 those having an associated frequency of occurrence over 20 years. We then run the in-
340 tegral volcanic plume model for each representative profile to obtain a probability dis-
341 tribution of the plume altitude using the frequency of occurrence of each profile (Fig-
342 ure 2 b). This distribution accounts for both variability in atmospheric conditions as sim-
343 ulated by one GCM within a 20-year period (e.g., due to seasonal cycle) and the inter-
344 GCM variability as we use a three-model ensemble.

345 In addition to plume height, for each characteristic profile identified by the SOM
346 algorithm, we estimate the tropopause height by interpolating the temperature profile
347 and finding the lowest altitude at which the temperature lapse rate is less than 2 K km^{-1} ,
348 for at least 2 km (following the World Meteorological Organization definition). Although
349 the vertical resolution of GCM datasets used is coarser than the multidecadal changes

350 in tropopause height, previous studies demonstrate that estimates on the basis of inter-
 351 polation of coarse temperature profiles are reliable to assess multidecadal changes in tropopause
 352 height (e.g., *Santer et al.* [2003]).

353 **3 Results**

354 To understand how global warming might impact the height reached by volcanic
 355 plumes, we first analyze distinct effects of projected changes in temperature and geopo-
 356 tential height profiles (which control the lapse rate), and horizontal wind speed profiles
 357 for 2 regions (one high-latitude, Chile, and one tropical, Philippines) under strong green-
 358 house gas forcing (scenario RCP8.5). We then assess the combined impacts of changes
 359 in temperature, geopotential height and wind for the same forcing and regions, and sum-
 360 marize results for all regions (Figure 1), periods (1981-2000, 2081-2100, 2181-2200 and
 361 2281-2300) and forcing scenarios (RCP2.6, RCP4.5 and RCP8.5). Finally, we illustrate
 362 our results by projecting changes in the height of historical eruptions if they were to oc-
 363 cur under future climate conditions.

364 **3.1 Impact of temperature and geopotential height changes under RCP8.5**

365 In this section, we fix the horizontal wind speed to the average of the reference pe-
 366 riod (1981-2000) for each region. Figure 5 shows the temperature as a function of geopo-
 367 tential height in Chile (a) and in the Philippines (b), for the reference (1981-2000), 2081-
 368 2100 and 2281-2300 periods. For both regions, the temperature increases with time in
 369 the troposphere, decreases in the stratosphere, and the tropopause height increases. In
 370 the tropical region (Philippines), changes in median temperature and tropopause height
 371 from one period to another are large compared to the seasonal and inter-annual variabil-
 372 ity over each period. In contrast, the changes are smaller compared to variability in the
 373 high-latitude region (Chile), mostly because of the higher seasonality. Between the late
 374 23rd century and the reference period, the tropospheric lapse rate is projected to decrease
 375 by 0.9 K km^{-1} in the Philippines and by 0.4 K km^{-1} in Chile. The stratospheric lapse
 376 rate is projected to increase by $\simeq 1 \text{ K km}^{-1}$ on average between the tropopause and \simeq
 377 30 km altitude, which results in a slightly positive lapse rate in the lower stratosphere
 378 in Chile, for the 2281-2300 period (where the lapse rate is defined as $\Gamma = -\frac{dT}{dz}$).

379 Volcanic plume heights vary with projected temperature and geopotential height
 380 changes (Figure 5, panels c and d). In particular, where the lapse rate decreases, plume
 381 height decreases and vice-versa. In the Philippines, for mass eruption rates of order of
 382 magnitude 10^7 kg s^{-1} , plume heights are projected to decrease by 2-3 km in the upper
 383 troposphere. Decrease in tropospheric plume height is weaker ($< 1 \text{ km}$) and less signif-
 384 icant in Chile. For both regions, stratospheric plume ($M_0 \gg 10^7 \text{ kg s}^{-1}$) heights are
 385 predicted to increase by $\simeq 2 \text{ km}$, with a more significant increase in the tropical region.
 386 The uncertainty in plume height due to temperature variability over one period is small
 387 ($\simeq 1\text{-}2 \text{ km}$ for both regions).

388 The ratio of the maximum plume altitude to the tropopause altitude (H^*) declines
 389 for both regions and all M_0 , as greenhouse gas forcing increases (Figure 5, panels e and
 390 f). In the Philippines, for an eruption whose median H^* was equal to 1 in the reference
 391 period, H^* decreases by 0.2-0.3 in 2281-2300. Similar changes are predicted for Chilean
 392 plumes, but are smaller and less significant due to relatively small decreases in tropo-
 393 spheric plume height and larger temperature variability. In the stratosphere, although
 394 plume heights increase, H^* decreases by $\simeq 0.2\text{--}0.3$ for both regions because the tropopause
 395 height increases over the same period.

396 **3.2 Impact of horizontal wind speed changes under RCP8.5**

397 We now fix the temperature and geopotential height to their average values for the
 398 reference period for each region while we apply daily wind profiles from GCM runs in
 399 the plume model. Overall, we observe no significant change in projected wind profiles
 400 in either region (Figure 6, panels a and b). For example, in Chile, there is a decrease in
 401 median tropospheric wind speed and an increase in median stratospheric wind speed.
 402 However, these changes are small relative to the wind variability over one period. Sim-
 403 ilar conclusions apply to the Philippines, where the winds are weaker and changes are
 404 smaller relative to Chile. For both regions, the wind speed variability in time increases
 405 with greenhouse gas forcing.

406 Variations of H^* (Figure 6, panels c and d) only reflect variations in plume height
 407 since the temperature profiles, and thus the tropopause height, are constant. For a given
 408 M_0 and over one period, wind variability causes H^* to vary by 0.1 to 0.4 around its me-

dian, which makes the changes in H^* driven by long-term wind speed changes in response to increasing greenhouse forcing negligible compared to these uncertainties.

3.3 Impact of combined changes of temperature, geopotential height and horizontal wind speed under RCP8.5

We now analyze the effect of combined changes in temperature, geopotential height and wind speed. To facilitate the discussion, we define a normalized mass eruption rate $M_0^* = \frac{M_0}{M_0^{tp,ref}}$, where $M_0^{tp,ref}$ is the median critical mass eruption rate for which $H^*=1$ for the reference period (1981-2000). Thus, our normalization for M_0 is dependent on the region, but indicates variations in M_0 required to reach the tropopause.

Figure 7 shows H^* as a function of M_0^* . Evolution of H^* as the greenhouse gas forcing increases is the same as when varying the temperature and geopotential height only (Figure 5). For a given M_0^* and period, uncertainties on H^* originating from variability of temperature, geopotential height and wind speed are comparable to those obtained when varying the wind speed only (Figure 6). For example, in the Philippines, the median H^* decreases by up to $\simeq 0.15$ in the upper troposphere, for the late 21st century, and up to $\simeq 0.25$ for the 23rd century (RCP8.5). Decrease of plume height and increase of tropopause height contribute equally to changes in H^* , and result in the increase of the critical mass eruption rate required to cross the tropopause. It is increased by a factor 1.65 for the late 21st century compared to the reference period, and a factor 2.8 for the 23rd century. We observe similar trends for Chile (Figure 7, left), although the magnitude of changes in H^* or critical M_0^* to reach the tropopause are smaller.

3.4 Summary: Results for all investigated regions, periods and scenarios

We summarize our results with two key values. The first is the median value of H^* for which $M_0^*=1$ (horizontal dotted lines in Figure 7; Table 3). The second is the median value of M_0^* for which $H^*=1$ (vertical dashed lines in Figure 7; Table 4). For the reference period, we estimate the 99% confidence interval on the median H^* for which $M_0^*=1$ or median M_0^* for which $H^*=1$ by using a bootstrap method (cf. Supporting Information S2).

438 For $M_0^*=1$, H^* mostly decreases by 0 to 0.25 relative to the 1981-2000 reference
 439 period (Table 3). For the RCP2.6 scenario, H^* increases by 0 to 0.03 in some extratrop-
 440 ical regions, and always decreases for tropical regions. Decreases in H^* are stronger and
 441 more statistically significant for tropical regions, higher RCP scenarios, and more dis-
 442 tant future for RCP4.5 and RCP8.5, for which the radiative forcing does not stabilize
 443 before 2300 (cf. Section 2.2 and *Van Vuuren et al.* [2011]). For RCP8.5, the median H^*
 444 reached with $M_0^*=1$ decreases by $\simeq 0.2$ in tropical regions and $\simeq 0.1$ in extra-tropical
 445 regions, compared to the reference period. Changes are statistically significant for all trop-
 446 ical regions and most extratropical regions for RCP8.5 and for tropical regions for RCP4.5.

447 Table 4 shows the median M_0^* for which $H^*=1$. The median critical mass eruption
 448 rate required to reach the tropopause generally increases by a factor up to 2.8 depend-
 449 ing on the region, period and scenario. As for Table 3, changes are more significant for
 450 tropical regions, stronger radiative forcing, and time periods further away in the future.
 451 In particular, for the RCP8.5 scenario, the critical mass eruption rate is increased by a
 452 factor 2 to 2.8 in tropical regions for the 22nd and 23rd centuries, and 1.25 to 2 in extra-
 453 tropical regions. Again, for this scenario, changes are statistically significant in all trop-
 454 ical regions and most extratropical regions. Values in Tables 3 and 4 are unchanged if
 455 we use the plume neutral buoyancy height H_b instead of the maximum plume height H
 456 (Figure 4) to define H^* .

457 3.5 Height projections for past eruptions

458 To illustrate the effects of changes in volcanic plume and tropopause height, we first
 459 test how the height of 13 historical eruptions (Table 2) would change relative to the tropopause
 460 height as a consequence of greenhouse gas emissions. For each eruption, Figure 8 shows
 461 H^* inferred from *Carn et al.* [2016] and predicted values for the 1981-2000 reference pe-
 462 riod, 2081-2100 (RCP8.5) and 2281-2300 (RCP8.5). Atmospheric conditions used to pre-
 463 dict H^* are associated with the region closest to the volcano considered except for the
 464 Etna eruption for which we retrieved reanalysis and GCM atmospheric profiles over Sicily
 465 (Figure 1, Table S2). Eruptions with H^* above 1 cross the tropopause. The observed
 466 H^* generally lies within the range predicted using GCM historical runs for the 1981-2000
 467 period. Predicted H^* for the late 21st century for the RCP8.5 scenario is lower than that
 468 which is predicted for the reference period. For 2 eruptions (El Chichón 1982 A and Mer-
 469 api 2010), the predicted median H^* is below 1, indicating that the probability that the

470 eruption will cross the tropopause is less than 50%. For the late 23rd century and a RCP8.5
 471 scenario, the median H^* for 4 eruptions is below 1, with a probability to cross the tropopause
 472 of less than 5% for El Chichón 1982 A and Merapi 2010. The El Chichón 1982 B and
 473 Pinatubo eruptions remain largely above the tropopause although H^* decreases for these
 474 eruptions as well. The value of H^* for analyzed basaltic eruptions also decreases. In par-
 475 ticular, our results suggest that a Laki-type eruption would have less than 50% chance
 476 of crossing the tropopause in between 2100 and 2300, under the RCP8.5 scenario.

477 Figure 8 illustrates the impact of global warming on different size and type of plumes,
 478 but does not reflect that smaller eruptive plumes (e.g., Merapi 2010) are more frequent
 479 than larger eruptive plumes (e.g., Pinatubo 1991). Accordingly, we project H^* for the
 480 subset of eruptions from the *Carn et al.* [2016] dataset described in Section 2.1 (i.e., in
 481 particular, $VEI \geq 3$ and observed $H^* \geq 0.5$). Figure 9 (panel (a)) shows the observed
 482 H^* and mass of injected SO_2 as a function of latitude and time. Panels (b)-(f) shows
 483 median H^* prediction under a 1981-2000, 2081-2100 and 2281-2300 climate (RCP4.5 and
 484 RCP8.5 for future periods). We show only stratospheric plumes (i.e., for which $H^* \geq$
 485 1) and indicate on each panel the corresponding estimate for the global and tropical vol-
 486 canic fluxes of SO_2 into the stratosphere. There is again a good agreement between H^*
 487 calculated from the *Carn et al.* [2016] dataset (Figure 9.a) and the values calculated for
 488 the reference period climate, using GCM historical runs (Figure 9.b). For the reference
 489 period, the total flux of volcanic SO_2 into the stratosphere is 1.26 Mt/yr, about 0.9 Mt/yr
 490 of which are injected in the tropics. Under a 2081-2100 climate evolving under a RCP4.5
 491 or RCP8.5 scenario, or 2281-2300 climate under RCP4.5, we find that there would be
 492 $\simeq 15$ -20 fewer eruptions reaching the stratosphere, on average, with most of the eruptions
 493 shifted below the tropopause being in the tropics. However, the flux of volcanic SO_2 into
 494 the stratosphere would only decrease by 0.04-0.06 Mt/yr (or 3 to 5%) for the total flux
 495 and 0.03-0.04 Mt/yr (or 3 to 4%) for the tropics. For a 2281-2300 climate under a RCP8.5
 496 scenario, $\simeq 40$ eruptions out of $\simeq 200$ in this dataset would be tropospheric rather than
 497 stratospheric. The corresponding reduction in the SO_2 injected into the stratosphere is
 498 0.22 Mt of SO_2 /yr (17%), 0.16 Mt of SO_2 /yr (18%) of which occurring in the tropics.
 499 Last, for eruptions that remain in the stratosphere, H^* decreases by 0.1-0.4 depending
 500 on the time period and scenario considered.

4 Discussion

4.1 Mechanisms driving changes in plume and tropopause heights

Under a RCP4.5 or RCP8.5 scenario, GCM projections imply that eruptions must have a larger mass eruption rate to reach the tropopause. This result is a consequence of: i) a decrease of tropospheric volcanic plume height and ii) an increase of the tropopause height. The decrease in tropospheric plume height is a consequence of the decrease in tropospheric temperature lapse rate (Figure 5). Indeed, there is a remarkable agreement between the decrease in plume height predicted by applying change in tropospheric temperature lapse rate in Equations 1 and 2, and decrease in plume height predicted by our volcanic plume model using daily profiles of temperature, wind speed and relative humidity. When fixing temperature profiles but varying horizontal wind speed (Figure 6), we observe no large change in the median plume height but an increased difference between the 5th and 95th quantile of plume height probability distribution. Horizontal wind speed is thus a source of uncertainty on plume height for a particular eruption, but multidecadal changes in wind speed in response to greenhouse gas emissions do not drive any significant shift of the plume height probability distribution. Our results apply to both explosive silicic eruptions plumes and thermal plumes related to basaltic eruptions (Figure 8).

Although our results rely on GCM predictions, they require only a decrease of tropospheric lapse rate and an increase of the tropopause height. Both CMIP5 GCMs and observations exhibit a decrease of the tropospheric temperature lapse rate in the tropics, over the 1960-2010 period [*Fu et al.*, 2011; *Simmons et al.*, 2014; *Sherwood and Nis- hant*, 2015]. In particular, CMIP5 GCMs simulate well the shape of warming rate profiles in the tropical troposphere, which controls the change in lapse rate [*Mitchell et al.*, 2013]. Also, an increase of the tropopause height is found consistently in GCMs and observations (e.g., [*Santer et al.*, 2003]).

A key question is to assess how past changes in temperature lapse rate and tropopause height have impacted the rise of volcanic plumes. *Glaze et al.* [2015] discuss how the height of a plume produced by a flood basalt eruption would change in an atmosphere typical of the Miocene. They suggest that a warmer atmosphere would cause a decrease in plume height. The near-vent atmospheric temperature controls the temperature difference between the erupted ash-gas mixture and the atmosphere, and thus the plume source buoy-

533 ancy flux. However, near the vent, the plume is hundreds of degrees Kelvin warmer than
534 the atmosphere and the source buoyancy flux would thus not be significantly affected
535 by a few-degrees Kelvin change of the atmospheric temperature. In addition, the plume
536 height only weakly depends on the plume source buoyancy flux relative to the atmospheric
537 stratification (Equation 1). A change in the mean tropospheric temperature without a
538 change in the lapse rate would also affect the stratification (Equation 2) but again it would
539 be negligible as atmospheric temperature is of order hundreds of degrees Kelvin.

540 **4.2 Sensitivity analysis**

541 In this section we test the sensitivity of our results to the choice of GCM (section
542 2.2.2) and to the entrainment coefficient values applied in our volcanic plume model (sec-
543 tion 2.3). We also briefly discuss the sensitivity of our results to the parameterization
544 of water droplet condensation in the model and the sensitivity to variability in eruption
545 source conditions other than the mass eruption rate.

546 **4.2.1 Choice of GCMs**

547 We analyze how our results differ when using an individual GCM of the ELT3 en-
548 semble (BCC-CSM-LR, CanESM2 and MPI-ESM-LR) relative to the results when their
549 ensemble was used. Figure 10 shows H^* as a function of M_0^* for the Philippines, for the
550 3 individual GCMs and the ensemble ELT3, for the reference period and the late 21st
551 and 23rd century for the RCP8.5 scenario. First, on the basis of our volcanic plume model,
552 all GCM projections result in a decrease of H^* and an increase of the critical mass erup-
553 tion rate required to reach the tropopause. For the 2081-2100 period, BCC-CSM-LR,
554 CanESM2 and MPI-ESM-LR predict an increase by a factor 1.35, 1.34 and 1.55 of the
555 critical mass eruption rate required to reach the tropopause, all significant at the 99%
556 confidence level. For the 2281-2300 period, BCC-CSM-LR and MPI-ESM-LR predict an
557 increase by a factor 1.99 and 3.16, respectively, both being significant again. An extended
558 (2100-2300) RCP8.5 run of the CanESM2 model was not available.

559 All three GCMs we use and their ensemble (ELT3) thus show similar trends and
560 differences in the results do not change our conclusions. Although using an ensemble with
561 more GCMs would make our analysis more complete statistically, we are limited by the
562 availability of extended RCP runs with daily outputs (Table S1). For similar reasons,

563 we also use a single run from each model. However, when comparing results using 1 or
 564 3 runs for historical experiments for the CanESM2 and MPI-ESM-LR, we did not find
 565 any significant difference. Finally, it is important to stress that 2 out of the 3 GCMs used
 566 (MPI-ESM-LR and CanESM2) are among the better performing GCMs according to the
 567 evaluation metrics tested in section 2.2.2, which gives greater confidence in our results.

568 **4.2.2 Volcanic plume model parameters**

569 In integral volcanic plume models, the values of the entrainment coefficients α and
 570 β (Equation 4), which govern the mixing of atmosphere into the volcanic plume, must
 571 be assigned. Entrainment coefficients are identified as the main source of uncertainties
 572 on the plume height (e.g., *Costa et al.* [2016]). To test the sensitivity of our results to
 573 entrainment coefficients, we show H^* as a function of M_0^* for the Philippines and for a
 574 RCP8.5 scenario, for the 6 different cases for entrainment coefficients (Figure 11). We
 575 obtain similar results when the ratio of entrainment coefficients $\frac{\beta}{\alpha}$ is kept constant ("Stan-
 576 dard", "Weak" and "Strong" entrainment rates cases corresponding to panels (a), (b) and
 577 (c) of Figure 11). When the ratio $\frac{\beta}{\alpha}$ is increased ("Weak radial entrainment rates", panel
 578 (d) of Figure 11), uncertainties on H^* induced by wind are larger and changes of H^* are
 579 slightly less statistically significant. This behavior is expected as the dependence of the
 580 plume height on wind is increased when increasing $\frac{\beta}{\alpha}$. In contrast, when the ratio $\frac{\beta}{\alpha}$ is
 581 decreased ("Strong radial entrainment rate", panel (e) of Figure 11), the significance of
 582 the changes slightly increases. Finally, we test the sensitivity of the results to the ran-
 583 dom choice of values for the entrainment coefficients, because entrainment coefficients
 584 depend on the plume dynamics and might vary between eruptions ("Variable entrain-
 585 ment rates", panel (f) of Figure 11). In this case, despite the increase by $\simeq 50\%$ of the
 586 upper bound uncertainty in H^* , the median H^* undergoes negligible change. The in-
 587 crease in the median critical mass eruption rate required to reach the tropopause is thus
 588 not sensitive to the value of entrainment coefficients used in the integral volcanic plume
 589 model; e.g., it varies between 2.71 and 3.02 for the 6 cases investigated and is always sig-
 590 nificant at the 99% level for 2281-2300.

591 **4.2.3 Additional factors affecting the height of volcanic plumes**

592 The release of latent heat caused by condensation of entrained water vapor can in-
 593 crease volcanic plume heights, which is discussed in Supporting Information (Figure S1).

594 The impact of changes in atmospheric humidity projected by GCMs largely depends on
 595 the condensation rate λ used in the integral volcanic plume model (see Section 2.3 and
 596 Table 1). For the end-member case $\lambda=0.098 \text{ s}^{-1}$ (large condensation rate), the median
 597 plume height of tropospheric plume and uncertainties on plume height increase, espe-
 598 cially in tropical regions. However, for tropical regions, the increase of the median mass
 599 eruption rate required to reach the tropopause differs negligibly from the model results
 600 that do not consider the condensation effect ($\lambda=0$) and remain significant at the 99%
 601 level for a RCP8.5 scenario. In addition to the mass eruption rate, plume height is in-
 602 fluenced by other source conditions. We test how the source temperature and gas con-
 603 tent as well as the vent altitude impact our results in Supporting Information (Figure
 604 S2). Among these three factors, uncertainty in the vent altitude is the main factor in-
 605 creasing uncertainty on plume height, but this does not affect our conclusions.

606 **4.3 Implications for future volcanic forcing**

607 Changes in volcanic plume height and tropopause height could have significant im-
 608 plications for future volcanic forcing as the longevity of volcanic aerosol-radiation inter-
 609 actions depends strongly on whether volcanic SO_2 is injected directly into the strato-
 610 sphere. The dispersal of volcanic particles also depends on plume height and wind speed
 611 and direction (e.g., *Burden et al.* [2011]). A combined variation of all these parameters
 612 could have a significant effect on the distributions of the associated hazards. In addition,
 613 atmospheric conditions also have a significant effect on plume dynamics and, therefore,
 614 on the occurrence of associated hazardous processes (e.g., buoyant plume versus pyro-
 615 clastic density currents, *Degruyter and Bonadonna* [2013]). Although we acknowledge
 616 that these are key issues that should be explored in detail in the future, we only discuss
 617 the implications of our results for future volcanic forcing in this study.

618 **4.3.1 Volcanic SO_2 injection efficiency metric**

619 The potential decrease of H^* by $\simeq 5 - 25\%$ relative to 1981-2000 (for a RCP4.5
 620 or RCP8.5 scenario, in the coming three centuries) has significant implications for plumes
 621 ascending to an altitude just a few kilometers above the tropopause. Although eruptions
 622 associated with these small plumes generally inject relatively moderate quantities of SO_2
 623 into the stratosphere (Table 2), they have a significant footprint on climate [*Solomon et al.*,
 624 2011; *Santer et al.*, 2014, 2015] and are more frequent than the eruptions associated with

625 very tall plumes [Brown *et al.*, 2014]. A generic SO₂ injection efficiency metric account-
 626 ing for both the quantity of SO₂ injected and the height of injection is a useful tool to
 627 further parameterize or characterize the impact of climate change on volcanic aerosol-
 628 radiation interactions. We propose this injection efficiency to be of the form:

$$629 \quad \eta_{SO_2} = \int_{M_c^*}^{\infty} \bar{n}_{SO_2} M_0^* f(M_0^*) dM_0^* . \quad (5)$$

630 Here \bar{n}_{SO_2} is the ratio of the mass of SO₂ injected by an eruption and its normalized mass
 631 eruption rate M_0^* , which is assumed to be a constant, $f(M_0^*)$ is the time-averaged fre-
 632 quency of an eruption of mass eruption rate M_0^* , and M_c^* is the critical normalized mass
 633 eruption rate required to reach the tropopause and is equal to 1 for the reference period
 634 by definition of M_0^* . Climate controls η_{SO_2} by governing M_c^* , whereas crustal magmatic
 635 processes might control $f(M_0^*)$ over time scales of 10² to 10⁴ years, and magmatism re-
 636 lated to mantle dynamics and plate tectonics enter at time scales of order > 10⁶ years.

637 To estimate η_{SO_2} for the reference period, we take \bar{n}_{SO_2} to be the average value
 638 of the ratio of the mass of SO₂ injected by an eruption to its normalized mass eruption
 639 rate M_0^* in the Carn *et al.* [2016] dataset. To estimate $f(M_0^*)$, we use the Carn *et al.*
 640 [2016] dataset for the frequent eruptions injecting less than $\simeq 3$ Mt of SO₂ that contribute
 641 to aerosol background. We use the ? dataset for intermittent events injecting more than
 642 $\simeq 3$ Mt of SO₂. Figure S3 shows the distribution of erupted mass of SO₂ from both datasets,
 643 to which we fit $f(M_0^*)$ using a Kernel distribution. Figure 12 (a) shows the estimated
 644 values of η_{SO_2} as a function of M_c^* . Using $M_c^*=1$, we find $\eta_{SO_2}=1.45$ Mt/yr for the ref-
 645 erence period, which is close to the value of 1.23 Mt/yr estimated in Figure 9 using the
 646 Carn *et al.* [2016] dataset only. To estimate η_{SO_2} for an arbitrary period, we use Equa-
 647 tion 1. Let r_T be the ratio of the tropopause height of the period considered to the tropopause
 648 height of the reference period. Let r_N be the ratio of the Brunt-Väisälä frequencies for
 649 the same periods. Then, using Equations 1, $M_c^* = r_T^4 r_N^3$. Figure 12 shows this scaling-
 650 based estimate of η_{SO_2} for a RCP4.5 and RCP8.5 scenario. Using average changes in trop-
 651 ical tropopause height and tropospheric temperature lapse rate to calculate M_c^* , we find
 652 $\eta_{SO_2}=1.34$ Mt/yr and $\eta_{SO_2}=1.31$ Mt/yr for the late 21st century for the RCP4.5 and
 653 RCP8.5 scenarios respectively, and $\eta_{SO_2}=1.23$ Mt/yr and $\eta_{SO_2}=1.0$ Mt/yr for the late
 654 23rd century for the same scenarios (Figure 12 (a)). Relative decreases in the volcanic
 655 injection of SO₂ into the stratosphere using this simple, scaling based approach are thus
 656 remarkably close to the ones estimated in Figure 9.

4.3.2 *Magnitude and likelihood of projected changes in volcanic SO₂ fluxes into the stratosphere*

Estimates of η_{SO_2} on the basis of either the scaling-based approach of Section 4.3.1 or from Figure 9 rely on several assumptions. In particular, estimates from Figure 9 assume that: (i) the 1980-2015 sequence of eruptions will be repeated in the future; (ii) all volcanic SO₂ is injected at the maximum plume altitude; and (iii) the plume altitude is the median altitude for the considered period and RCP scenario. In addition, we use a steady-state plume model, which can not account for the potential additional transport of SO₂ across the tropopause by atmospheric circulation (e.g., Bourassa *et al.* [2012]) or by natural convection after absorption and warming (e.g., de Laat *et al.* [2012]).

In a preliminary effort to relax some of these assumptions, we use a Monte Carlo method to estimate future stratospheric injection of volcanic SO₂ over a century, for a specified time period and forcing scenario. For one simulation, we randomly sample 36525 days (100 years) in the 1980-2015 period, which is the longest period with available plume height and SO₂ loading for most eruptions. For each day corresponding to an eruption in the Carn *et al.* [2016] dataset injecting less than 3 Mt of SO₂, we assume that an eruption occurs with the following characteristics:

- The region and vent altitude is the same as for the original eruption.
- The mass eruption rate is $10^\psi \times M_{Carn}$ where M_{Carn} is the mass eruption rate of the original eruption and ψ is a random number between -0.3 and 0.3. Since $10^{0.3} \simeq 2$, the resulting mass eruption rate is within a factor 2 of the one of the original eruption. This approach enables us to randomize the mass eruption rate, while preserving its order of magnitude such that the distribution of mass eruption rates is similar to the one inferred for the 1980-2015 period.
- The mass of SO₂ is $10^\phi \times MSO2_{Carn}$ where $MSO2_{Carn}$ is the mass of SO₂ of the original eruption and ϕ is a random number between -0.3 and 0.3, where the choice of random number range is based on the same argument as for the mass eruption rate.
- Atmospheric conditions correspond to a day randomly sampled from the GCM ensemble, for the specified period and scenario.
- The SO₂ is uniformly distributed between H_b and $2H - H_b$ where H is the maximum plume altitude and H_b the altitude of neutral buoyancy of the plume. This

689 approach is approximately equivalent to distributing the SO₂ over a layer of height
 690 30-50% of the maximum height. For a steady plume and in the absence of addi-
 691 tional vertical transport by atmospheric winds or thermal convection, we would
 692 have distributed the SO₂ in a layer of thickness $H-H_b$. Here we arbitrarily dou-
 693 ble this thickness to explore a larger vertical spread of the SO₂ due to unstead-
 694 iness and spreading mechanisms mentioned above. The chosen layer thickness is
 695 coherent with uncertainties on observed plume height shown on Figure 8, which
 696 are due to a large extent to unsteadiness of the eruption, or uncertainties related
 697 to vertical transport of the plume.

698 Last, we randomly sample a 100-year period in the ? dataset from which we excluded
 699 eruptions injecting less than 3 Mt of SO₂. We assume that corresponding sampled erup-
 700 tions inject SO₂ directly into the stratosphere, regardless of atmospheric conditions.

701 We perform 300 Monte Carlo simulations of 100 years of volcanic eruptions for the
 702 late 21st and late 23rd centuries for RCP4.5 and RCP8.5 scenarios, as well as for the ref-
 703 erence period. Results are not sensible to the number of simulations performed for more
 704 than $\simeq 100$ simulations. Figure 12 shows the median flux of SO₂ into the stratosphere
 705 η_{SO_2} (panel (d)) as well as the median global (panel(c)) and tropical (panel(b)) flux of
 706 volcanic SO₂ into the stratosphere due to small eruptions only (i.e., the ones injecting
 707 less than $\simeq 3$ Mt of SO₂ that are sampled from the *Carn et al.* [2016] dataset). The prob-
 708 ability for projected stratospheric fluxes of future time periods to be smaller than fluxes
 709 for the reference period is also reported on each panel.

710 Panel (c) (Figure 12) shows that the flux of SO₂ into the stratosphere related to
 711 small eruptions may decrease by $\simeq 5-25\%$ for a RCP4.5 or RCP8.5 scenario depending
 712 on the period considered. A decrease is “likely” (66 to 90% probability, using the IPCC
 713 AR5 likelihood scale, *Mastrandrea et al.* [2010]) by the 23rd century but “about as likely
 714 as not” (33 to 66% probability) for the 21st century due to large uncertainties related
 715 to future eruptive conditions. Projected decreases of the tropical flux of SO₂ carried by
 716 small eruptions (panel (b)) are larger ($\simeq 10-50\%$), and “likely” (66 to 90% probability)
 717 to “very likely” ($\geq 90\%$). However, panel (d) shows that the total flux, including the con-
 718 tribution from large eruptions, would undergo a smaller decrease ($\simeq 2-12\%$) that would
 719 be “about as likely as not” due to the large simulated variability in volcanic SO₂ fluxes

720 when including contribution from all eruptions. Reductions are even smaller and less likely
721 for a RCP2.6 scenario (not shown).

722 To summarize, our results suggest that global warming may significantly decrease
723 the background volcanic flux of SO₂ into the stratosphere sustained by small (≤ 3 Mt
724 of SO₂) and frequent (compared to the rate of decay of stratospheric sulfate aerosols)
725 stratospheric injections. However, the effect on the total flux of SO₂ into the stratosphere
726 is small because of the contributions of large (≥ 3 Mt of SO₂) and infrequent (compared
727 to the rate of decay of stratospheric sulfate aerosols) events. As a final remark on this
728 result, our view may be conservative because we assume that large eruptions inject SO₂
729 into the stratosphere regardless of climate, which is not the case at least for basaltic erup-
730 tions such as the 1783-1784 eruptions of Laki [*Thordarson and Self, 2003*] as shown in
731 Figure 8.

732 Critically, our estimates of a decrease of the flux of volcanic SO₂ into the strato-
733 sphere challenges the use of steady volcanic forcing for climate projections in two ways.
734 First, our results suggest a new positive feedback between climate and volcanic aerosol-
735 radiation interaction: (i) global warming decreases the frequency of eruptions with strato-
736 spheric injections; (ii) less frequent stratospheric volcanic injections result in a decrease
737 of the long-term average sulfate aerosol concentration in the stratosphere and thus of the
738 albedo of the atmosphere; and (iii) a reduced atmospheric albedo will enhance global warm-
739 ing. Assuming a long-term average volcanic forcing of small eruptions ($VEI \leq 5$) of
740 order of magnitude -0.1 W.m^{-2} [*Solomon et al., 2011*], and that the relative variations
741 in this average would be of the same order of magnitude as change in the average vol-
742 canic SO₂ flux into the stratosphere, the order of magnitude of this feedback would be
743 $10^{-2} \text{ W.m}^{-2}/^{\circ}\text{C}$. It may thus make a negligible contribution to global warming rate, al-
744 though we note that the order of magnitude of projected changes in stratospheric SO₂
745 flux is comparable to the increase in volcanic stratospheric SO₂ since 2002 which has been
746 argued to contribute to overestimates of global warming rate by GCMs (e.g., *Solomon*
747 *et al.* [2011]; *Santer et al.* [2014]). The proposed feedback may also prove important for
748 understanding the evolution of volcanic aerosol forcing in the future, as well as the over-
749 all impact of Earth's climate on the distribution of volcanic inputs in the atmosphere.
750 Second, our statistical analyses suggest that for a given climate, the average flux of vol-
751 canic SO₂ into the stratosphere over a century may vary by a factor $\simeq 5 - 10$, which

would likely have important consequences for forcing related to volcanic aerosol-radiation interactions and may increase uncertainties in future climate projections.

4.4 Limitations and potential improvements: beyond a binary view of volcanic aerosol forcing sensitivity to plume height

The discussion of our results is grounded in the assumption that only stratospheric aerosols exert a significant influence on global climate. Although this is a good first approximation, the shift in impact between a tropospheric and stratospheric injection of SO₂ is not as abrupt. The following considerations enter the full picture of volcanic forcing:

1. For stratospheric plumes, aerosol-radiation interactions are sensitive to the plume height, although most sensitivity studies focus on the impact of the eruption season and latitude. *Stoffel et al.* [2015] test the sensitivity of climate response to plume height for the Samalas 1257 eruption, and report larger aerosol optical depth and 40°N-90°N land temperature anomalies for an upper stratospheric injection (36-43 km) compared to a lower stratospheric injection (22-26 km), with differences by up to a factor $\simeq 2$ depending on the season. A sensitivity study for high latitude eruptions using a GCM coupled with a stratospheric chemistry/aerosols microphysics module suggests similar effects (Matthew Toohey, personal communication). For high latitude eruptions, aerosol clouds issued from stratospheric plumes smaller than the tropical tropopause spread along constant potential temperature surface and may thus cross the tropopause and be scavenged at mid latitudes [*Holton et al.*, 1995]. *Carn et al.* [2016], on the basis of satellite measurements, also shows that the e-folding time for SO₂ removal increases with the plume height, and suggests that H^* is the main parameter controlling the longevity of SO₂. Greater longevity for SO₂ may lead a slower aerosol production and to a reduced but longer lasting peak of volcanic aerosol-radiation interactions [*Timmreck*, 2012]. Thus, the decrease of H^* for large stratospheric plumes (Figures 7, 9) might have important consequences for future radiative forcing even if they are not shifted below the tropopause.
2. Tropospheric eruptive plumes also impact climate by increasing cloud condensation nuclei concentrations and, in turn, cloud reflectivity (aerosol-cloud interactions). For example, during the Bárðarbunga 2014-2015 eruption (Iceland), *Mc-*

783 *Coy and Hartmann* [2015] report increases of up to 2 W m^{-2} in the reflected so-
784 lar radiation, over the North Atlantic. *Schmidt et al.* [2012] estimate that the long
785 term average volcanic aerosol-cloud interactions forcing is $\simeq -0.3$ to -1.6 W m^{-2} ,
786 depending on the background aerosol concentrations). As aerosol and nucleated
787 cloud radiative properties depend on the height of injection of volcanic SO_2 in the
788 troposphere [*Schmidt et al.*, 2016], volcanic aerosol-cloud interactions may also de-
789 pend on the height of volcanic plumes. As a result, a larger injection of volcanic
790 SO_2 into the troposphere and the decrease of the height of tropospheric plumes
791 (Figure 8) may increase future volcanic aerosol-cloud interactions forcing, although
792 the projected increase in volcanic SO_2 flux into the troposphere is small ($\simeq 0$ –
793 5%, estimated from panel (c) of Figure 12 and tropospheric flux estimates from
794 *Halmer et al.* [2002] and *Carn et al.* [2016]).

- 795 3. An injection of SO_2 directly into the stratosphere may not be necessary for the
796 SO_2 or sulfur aerosol to reach the stratosphere and result in significant aerosol-
797 radiation interactions. Upper tropospheric volcanic sulfur gases or aerosols may
798 be transported to some extent through the tropopause by atmospheric circulation
799 [*Bourassa et al.*, 2012, 2013; *Clarisse et al.*, 2014] or by convection driven as a re-
800 sult of absorption of Earth and Sun radiation, which has been suggested for the
801 Black Sunday fire [*de Laat et al.*, 2012].
- 802 4. Even when a volcanic eruption produces a stable plume, part of the erupted ma-
803 terial may collapse to form pyroclastic flows [*Carazzo and Jellinek*, 2012]. Part
804 of the SO_2 lost to pyroclastic flows may however be entrained into co-ignimbrite
805 columns [*Woods and Wohletz*, 1991]. Although the height reached by co-ignimbrite
806 plumes are typically lower than the main plinian column with which they are as-
807 sociated, they may transport SO_2 into the stratosphere for very large eruptions
808 such as Tambora in 1815 or Pinatubo in 1991 [*Herzog and Graf*, 2010]. Such ef-
809 fects would not be captured by the model used in this study.

810 Different modeling approaches can be applied to tackle some of these four limita-
811 tions. For example, in order to estimate changes in volcanic aerosol-radiation interac-
812 tions, our plume model can provide SO_2 altitude and loading to an idealized volcanic
813 aerosol model, such as Easy Volcanic Aerosol [*Toohey et al.*, 2016b], or to a GCM cou-
814 pled with a stratospheric chemistry/aerosols microphysics module, such as MAECHAM5-
815 HAM (e.g., *Toohey et al.* [2011]). The use of a 3-dimensional plume model instead of an

816 integral volcanic plume model may enable to better account for the complexity of the
817 flows resulting from a volcanic eruptions, such as co-ignimbrite plumes.

818 As a final note to this discussion, global warming may impact volcanic aerosol forc-
819 ing via mechanisms different than the one proposed here. For example, the gradual melt-
820 ing of continental snow and ice cover implies that future eruptions are less likely to melt
821 and entrain surface water into the eruption plume, which may affect both the probabil-
822 ity of collapse of a plume [*Koyaguchi and Woods*, 1996] and the radiative forcing of the
823 eruption [*LeGrande et al.*, 2016]. Changes in atmospheric circulation may affect the dis-
824 tribution and e-folding time of stratospheric aerosols (e.g., *McLandress and Shepherd* [2009];
825 *Jones et al.* [2016]) and changes in water vapor may affect the aerosol size, and thus their
826 radiative properties and e-folding time (e.g., *Gottelman et al.* [2010]). Finally, a num-
827 ber of studies show that eruption frequency is impacted by continental ice-sheets, alpine
828 glacier or sea-level change (e.g. *Hall* [1982]; *McGuire et al.* [1997]; *Jellinek et al.* [2004]).
829 The response of volcanic aerosol forcing to these combined effects may improve our un-
830 derstanding of the evolution of volcanic aerosol forcing.

831 5 Conclusions

832 In this study, we investigate whether the ongoing global warming, driven by an-
833 thropogenic greenhouse gas emissions, will shift volcanic eruption plume height relative
834 to the tropopause height. We compute volcanic plume heights using an integral volcanic
835 plume model. Atmospheric conditions are obtained from an ensemble of GCM runs for
836 historical and RCP experiments.

837 We find that the critical mass eruption rate required to reach the tropopause will
838 increase as a consequence of: (i) a decrease in the heights of tropospheric plumes driven
839 by a decrease of the tropospheric temperature lapse rate; and (ii) an increase of the tropopause
840 height. This result is independent of the choice of GCMs and insensitive to parameter-
841 izations for the volcanic plume model. Depending on the latitudinal zone, RCP scenario
842 and time period considered, the critical mass eruption rate increases by up to a factor
843 of 2.8 relative to the late 20th century. This increase is significant in tropical regions for
844 a RCP4.5 scenario and all tested regions for a RCP8.5 scenario. This result implies that
845 eruptions rising a few kilometers above the tropopause under current climate conditions
846 may be shifted to the stratosphere in the future. As a consequence, we estimate that the

847 flux of SO₂ into the stratosphere associated to small (≤ 3 Mt of SO₂) frequent (compared
848 to the rate of decay of stratospheric sulfate aerosols) eruptions would likely decrease by
849 $\simeq 5 - 25\%$ over the next three centuries, for a RCP4.5 or RCP8.5 scenario. The am-
850 plitude and likelihood of such decrease is more pronounced for tropical injections. Due
851 to the contribution of large (≥ 3 Mt of SO₂) infrequent (compared to the rate of decay
852 of stratospheric volcanic aerosol) eruptions, and to large uncertainties in future eruptive
853 source conditions, the total flux of volcanic SO₂ into the stratosphere is projected to de-
854 crease by $\simeq 2 - 12\%$, with the likelihood of such decrease being weak. Finally, our re-
855 sults challenge the popular use of steady volcanic radiative forcing in climate projections
856 for the coming centuries. Instead, our work suggests that greenhouse gas driven climate
857 change will result in less cooling from volcanic eruptions, potentially resulting in a pos-
858 itive feedback. The expected amplitude for this feedback is small, although it has been
859 argued that the increase in stratospheric SO₂ injections since 2002, which amplitude are
860 comparable to the decrease projected in our study, has contributed to the overestima-
861 tion of global warming rate by GCMs (e.g., *Solomon et al.* [2011]; *Santer et al.* [2014]).
862 While processes linking eruptive source conditions to the distribution of volcanic SO₂
863 are neglected in past GCMs experiments on volcanic forcing (e.g., [*Stenchikov et al.*, 2006;
864 *Driscoll et al.*, 2012]) and in the next Model Intercomparison Project on the climatic re-
865 sponse to Volcanic forcing [*Zanchettin et al.*, 2016], we demonstrate that such processes
866 may prove critical to the understanding of past and future volcanic forcing.

867 **Acknowledgments**

868 The authors warmly thank Anja Schmidt, Alan Robock, Jim Haywood and Ben-
869 jamin Edwards who organized the Climate-Volcano Feedbacks sessions VS32/33 at the
870 International Union of Geodesy and Geophysics 2016, which motivated this work. This
871 work benefited from very useful discussions with Matthew Toohey and all participants
872 of the Volcanic Impacts on Climate and Society 2016 workshop. We thank the editor,
873 associate editor, and three anonymous reviewers for their thorough comments and sug-
874 gestions which greatly improved the original manuscript. Thomas J. Aubry acknowledges
875 funding from the University of British Columbia through a Four Year Fellowship. Thomas
876 J. Aubry and A. Mark Jellinek were supported by Natural Sciences and Engineering Re-
877 search Council of Canada during completion of this work. Costanza Bonadonna was sup-
878 ported by the Swiss National Science Foundation (project number 200021_156255). We

879 acknowledge the World Climate Research Programme's Working Group on Coupled Mod-
880 eling, which is responsible for CMIP, and we thank the climate modeling groups for pro-
881 ducing and making available their model output. We thank the NOAA/OAR/ESRL/PSD
882 and the ECMWF for making reanalysis data available. We thank Simon A. Carn and
883 the National Aeronautics and Space Administration Goddard Earth Sciences Data and
884 Information Services Center for making available the Multi-Satellite Volcanic Sulfur Diox-
885 ide Database Long-Term. We acknowledge the Smithsonian Institution Global Volcan-
886 ism Program for compiling the Holocene volcanoes database. We thank the Laboratory
887 of Computer and Information Science for making the SOM toolbox v2.0 freely available
888 on
889 <http://www.cis.hut.fi/projects/somtoolbox/>.

890 References

- 891 Bonadonna, C., M. Pistolesi, R. Cioni, W. Degruyter, M. Elissondo, and V. Bau-
892 mann (2015), Dynamics of wind-affected volcanic plumes: The example of the
893 2011 Cordón Caulle eruption, Chile, *Journal of Geophysical Research: Solid Earth*,
894 *120*(4), 2242–2261, doi:10.1002/2014JB011478.
- 895 Bourassa, A. E., A. Robock, W. J. Randel, T. Deshler, L. A. Rieger, N. D. Lloyd,
896 E. T. Llewellyn, and D. A. Degenstein (2012), Large volcanic aerosol load in the
897 stratosphere linked to asian monsoon transport, *Science*, *337*(6090), 78–81, doi:
898 10.1126/science.1219371.
- 899 Bourassa, A. E., A. Robock, W. J. Randel, T. Deshler, L. A. Rieger, N. D. Lloyd,
900 E. Llewellyn, and D. A. Degenstein (2013), Response to comments on "large vol-
901 canic aerosol load in the stratosphere linked to asian monsoon transport", *Science*,
902 *339*(6120), 647–647, doi:10.1126/science.1227961.
- 903 Brown, S. K., H. S. Crossweller, R. S. J. Sparks, E. Cottrell, N. I. Deligne, N. O.
904 Guerrero, L. Hobbs, K. Kiyosugi, S. C. Loughlin, L. Siebert, et al. (2014), Char-
905 acterisation of the Quaternary eruption record: analysis of the large magnitude
906 explosive volcanic eruptions (LaMEVE) database, *Journal of Applied Volcanology*,
907 *3*(1), 1–22, doi:10.1186/2191-5040-3-5.
- 908 Brühl, C., J. Lelieveld, H. Tost, M. Höpfner, and N. Glatthor (2015), Stratospheric
909 sulfur and its implications for radiative forcing simulated by the chemistry climate
910 model EMAC, *Journal of Geophysical Research: Atmospheres*, *120*(5), 2103–2118,

911 doi:10.1002/2014JD022430.

912 Burden, R. E., J. C. Phillips, and T. K. Hincks (2011), Estimating volcanic plume
 913 heights from depositional clast size, *Journal of Geophysical Research: Solid Earth*,
 914 *116*(B11), doi:10.1029/2011JB008548.

915 Bursik, M. (2001), Effect of wind on the rise height of volcanic plumes, *Geophysical*
 916 *Research Letters*, *28*, 3821–3824, doi:10.1029/2001GL013393.

917 Carazzo, G., and A. M. Jellinek (2012), A new view of the dynamics, stability and
 918 longevity of volcanic clouds, *Earth and Planetary Science Letters*, *325–326*, 39–51,
 919 doi:10.1016/j.epsl.2012.01.025.

920 Carazzo, G., F. Girault, T. J. Aubry, H. Bouquerel, and E. Kaminski (2014), Lab-
 921 oratory experiments of forced plumes in a density-stratified crossflow and impli-
 922 cations for volcanic plumes, *Geophysical Research Letters*, *41*(24), 8759–8766,
 923 doi:10.1002/2014GL061887.

924 Carn, S., L. Clarisse, and A. Prata (2016), Multi-decadal satellite measurements of
 925 global volcanic degassing, *Journal of Volcanology and Geothermal Research*, *311*,
 926 99–134, doi:10.1016/j.jvolgeores.2016.01.002.

927 Chylek, P., J. Li, M. Dubey, M. Wang, and G. Lesins (2011), Observed and model
 928 simulated 20th century Arctic temperature variability: Canadian earth system
 929 model CanESM2, *Atmospheric Chemistry and Physics Discussions*, *11*(8), 22,893–
 930 22,907, doi:10.5194/acpd-11-22893-2011.

931 Clarisse, L., P.-F. Coheur, N. Theys, D. Hurtmans, and C. Clerbaux (2014), The
 932 2011 Nabro eruption, a SO₂ plume height analysis using IASI measurements, *At-*
 933 *mospheric chemistry and physics*, *14*(6), 3095–3111, doi:10.5194/acp-14-3095-2014.

934 Collins, M., R. Knutti, J. Arblaster, J.-L. Dufresne, T. Fichefet, P. Friedling-
 935 stein, X. Gao, W. Gutowski, T. Johns, G. Krinner, M. Shongwe, C. Tebaldi,
 936 A. Weaver, and M. Wehner (2013a), *Long-term Climate Change: Projections,*
 937 *Commitments and Irreversibility*, book section 12, pp. 1029–1136, Cambridge
 938 University Press, Cambridge, United Kingdom and New York, NY, USA, doi:
 939 10.1017/CBO9781107415324.024.

940 Collins, M., R. Knutti, J. Arblaster, J.-L. Dufresne, T. Fichefet, P. Friedling-
 941 stein, X. Gao, W. Gutowski, T. Johns, G. Krinner, M. Shongwe, C. Tebaldi,
 942 A. Weaver, and M. Wehner (2013b), *Long-term Climate Change: Projections,*
 943 *Commitments and Irreversibility*, book section 12, pp. 1029–1136, Cambridge

- 944 University Press, Cambridge, United Kingdom and New York, NY, USA, doi:
 945 10.1017/CBO9781107415324.024.
- 946 Costa, A., Y. Suzuki, M. Cerminara, B. Devenish, T. E. Ongaro, M. Herzog, A. V.
 947 Eaton, L. Denby, M. Bursik, M. de' Michieli Vitturi, S. Engwell, A. Neri, S. Bar-
 948 sotti, A. Folch, G. Macedonio, F. Girault, G. Carazzo, S. Tait, E. Kaminski,
 949 L. Mastin, M. Woodhouse, J. Phillips, A. Hogg, W. Degruyter, and C. Bonadonna
 950 (2016), Results of the eruptive column model inter-comparison study, *Journal of*
 951 *Volcanology and Geothermal Research*, doi:10.1016/j.jvolgeores.2016.01.017.
- 952 de Laat, A. T. J., D. C. Stein Zweers, R. Boers, and O. N. E. Tuinder (2012), A
 953 solar escalator: Observational evidence of the self-lifting of smoke and aerosols
 954 by absorption of solar radiation in the February 2009 Australian Black Sat-
 955 urday plume, *Journal of Geophysical Research: Atmospheres*, 117(D4), doi:
 956 10.1029/2011JD017016, d04204.
- 957 Degruyter, W., and C. Bonadonna (2012), Improving on mass flow rate es-
 958 timates of volcanic eruptions, *Geophysical Research Letters*, 39(16), doi:
 959 10.1029/2012GL052566.
- 960 Degruyter, W., and C. Bonadonna (2013), Impact of wind on the condition for
 961 column collapse of volcanic plumes, *Earth and Planetary Science Letters*, 377,
 962 218–226, doi:10.1016/j.epsl.2013.06.041.
- 963 Driscoll, S., A. Bozzo, L. J. Gray, A. Robock, and G. Stenchikov (2012), Coupled
 964 Model Intercomparison Project 5 (CMIP5) simulations of climate following vol-
 965 canic eruptions, *Journal of Geophysical Research: Atmospheres*, 117(D17), doi:
 966 10.1029/2012JD017607.
- 967 Flato, G., J. Marotzke, B. Abiodun, P. Braconnot, S. Chou, W. Collins, P. Cox,
 968 F. Driouech, S. Emori, V. Eyring, C. Forest, P. Gleckler, E. Guilyardi, C. Jakob,
 969 V. Kattsov, C. Reason, and M. Rummukainen (2013), *Evaluation of Climate Mod-*
 970 *els*, book section 9, pp. 741–866, Cambridge University Press, Cambridge, United
 971 Kingdom and New York, NY, USA, doi:10.1017/CBO9781107415324.020.
- 972 Folch, A., A. Costa, and G. Macedonio (2016), FPLUME-1.0: An integral volcanic
 973 plume model accounting for ash aggregation, *Geoscientific Model Development*,
 974 9(1), 431, doi:10.5194/gmd-9-431-2016.
- 975 Fromm, M., G. Nedoluha, and Z. Charvát (2013), Comment on "Large volcanic
 976 aerosol load in the stratosphere linked to asian monsoon transport", *Science*,

- 977 339(6120), 647–647, doi:10.1126/science.1228605.
- 978 Fu, Q., S. Manabe, and C. M. Johanson (2011), On the warming in the tropical
979 upper troposphere: Models versus observations, *Geophysical Research Letters*,
980 38(15), doi:10.1029/2011GL048101.
- 981 Gettelman, A., M. I. Hegglin, S.-W. Son, J. Kim, M. Fujiwara, T. Birner,
982 S. Kremser, M. Rex, J. A. Añel, H. Akiyoshi, J. Austin, S. Bekki, P. Braesike,
983 C. Brühl, N. Butchart, M. Chipperfield, M. Dameris, S. Dhomse, H. Garny, S. C.
984 Hardiman, P. Jöckel, D. E. Kinnison, J. F. Lamarque, E. Mancini, M. Marc-
985 hand, M. Michou, O. Morgenstern, S. Pawson, G. Pitari, D. Plummer, J. A. Pyle,
986 E. Rozanov, J. Scinocca, T. G. Shepherd, K. Shibata, D. Smale, H. Teysse, and
987 W. Tian (2010), Multimodel assessment of the upper troposphere and lower
988 stratosphere: Tropics and global trends, *Journal of Geophysical Research: Atmo-
989 spheres*, 115(D3), doi:10.1029/2009JD013638, d00M08.
- 990 Giorgetta, M. A., J. Jungclaus, C. H. Reick, S. Legutke, J. Bader, M. Böttinger,
991 V. Brovkin, T. Crueger, M. Esch, K. Fieg, et al. (2013), Climate and carbon cycle
992 changes from 1850 to 2100 in MPI-ESM simulations for the Coupled Model In-
993 tercomparison Project phase 5, *Journal of Advances in Modeling Earth Systems*,
994 5(3), 572–597, doi:10.1002/jame.20038.
- 995 Glaze, L. S., S. M. Baloga, and L. Wilson (1997), Transport of atmospheric water
996 vapor by volcanic eruption columns, *Journal of Geophysical Research: Atmo-
997 spheres*, 102(D5), 6099–6108, doi:10.1029/96JD03125.
- 998 Glaze, L. S., S. Self, A. Schmidt, and S. J. Hunter (2015), Assessing eruption col-
999 umn height in ancient flood basalt eruptions, *Earth and Planetary Science Letters*,
1000 doi:10.1016/j.epsl.2014.07.043.
- 1001 Gleckler, P. J., K. E. Taylor, and C. Doutriaux (2008), Performance metrics for
1002 climate models, *Journal of Geophysical Research: Atmospheres*, 113(D6), doi:
1003 10.1029/2007JD008972.
- 1004 Guo, S., G. J. S. Bluth, W. I. Rose, I. M. Watson, and A. J. Prata (2004), Re-
1005 evaluation of SO₂ release of the 15 June 1991 Pinatubo eruption using ultraviolet
1006 and infrared satellite sensors, *Geochemistry, Geophysics, Geosystems*, 5(4), doi:
1007 10.1029/2003GC000654.
- 1008 Hall, K. (1982), Rapid deglaciation as an initiator of volcanic activity: An
1009 hypothesis, *Earth Surface Processes and Landforms*, 7(1), 45–51, doi:

- 1010 10.1002/esp.3290070106.
- 1011 Halmer, M., H.-U. Schmincke, and H.-F. Graf (2002), The annual volcanic gas in-
 1012 put into the atmosphere, in particular into the stratosphere: a global data set for
 1013 the past 100 years, *Journal of Volcanology and Geothermal Research*, *115*(3–4),
 1014 511–528, doi:10.1016/S0377-0273(01)00318-3.
- 1015 Hartmann, D., A. Klein Tank, M. Rusticucci, L. Alexander, S. Brönnimann,
 1016 Y. Charabi, F. Dentener, E. Dlugokencky, D. Easterling, A. Kaplan, B. Soden,
 1017 P. Thorne, M. Wild, and P. Zhai (2013), *Observations: Atmosphere and Surface*,
 1018 book section 2, pp. 159–254, Cambridge University Press, Cambridge, United
 1019 Kingdom and New York, NY, USA, doi:10.1017/CBO9781107415324.008.
- 1020 Haywood, J. M., A. Jones, and G. S. Jones (2014), The impact of volcanic erup-
 1021 tions in the period 2000–2013 on global mean temperature trends evaluated in
 1022 the HadGEM2-ES climate model, *Atmospheric Science Letters*, *15*(2), 92–96,
 1023 doi:10.1002/asl2.471.
- 1024 Herzog, M., and H.-F. Graf (2010), Applying the three-dimensional model ATHAM
 1025 to volcanic plumes: Dynamic of large co-ignimbrite eruptions and associated
 1026 injection heights for volcanic gases, *Geophysical Research Letters*, *37*(19), doi:
 1027 10.1029/2010GL044986, 119807.
- 1028 Hewett, T., J. Fay, and D. Hoult (1971), Laboratory experiments of smokestack
 1029 plumes in a stable atmosphere, *Atmospheric Environment*, *5*, 767–789.
- 1030 Holton, J. R., P. H. Haynes, M. E. McIntyre, A. R. Douglass, R. B. Rood, and
 1031 L. Pfister (1995), Stratosphere-troposphere exchange, *Reviews of geophysics*,
 1032 *33*(4), 403–439, doi:10.1029/95RG02097.
- 1033 Iles, C., and G. Hegerl (2015), Systematic change in global patterns of stream-
 1034 flow following volcanic eruptions, *Nature Geoscience*, *8*(11), 838–842, doi:
 1035 10.1038/ngeo2545.
- 1036 Jellinek, A. M., M. Manga, and M. O. Saar (2004), Did melting glaciers cause
 1037 volcanic eruptions in eastern California? Probing the mechanics of dike
 1038 formation, *Journal of Geophysical Research: Solid Earth*, *109*(B9), doi:
 1039 10.1029/2004JB002978, b09206.
- 1040 Jones, A. C., J. M. Haywood, A. Jones, and V. Aquila (2016), Sensitivity of vol-
 1041 canic aerosol dispersion to meteorological conditions: A pinatubo case study,
 1042 *Journal of Geophysical Research: Atmospheres*, *121*(12), 6892–6908, doi:

- 1043 10.1002/2016JD025001.
- 1044 Kalnay, E., M. Kanamitsu, R. Kistler, W. Collins, D. Deaven, L. Gandin, M. Iredell,
 1045 S. Saha, G. White, J. Woolen, Y. Zhu, M. Chelliah, W. Ebisuzaki, W. Higgins,
 1046 et al. (1996), The NCEP/NCAR 40-year reanalysis project, *Bulletin of the Ameri-*
 1047 *can Meteorological Society*, 77(3), 437–471, doi:10.1175/1520-0477(1996)077.
- 1048 Kohonen, T. (1982), Self-organized formation of topologically correct feature maps,
 1049 *Biological cybernetics*, 43(1), 59–69, doi:10.1007/BF00337288.
- 1050 Koyaguchi, T., and A. W. Woods (1996), On the formation of eruption columns
 1051 following explosive mixing of magma and surface-water, *Journal of Geophysical*
 1052 *Research: Solid Earth*, 101(B3), 5561–5574, doi:10.1029/95JB01687.
- 1053 LeGrande, A. N., K. Tsigaridis, and S. E. Bauer (2016), Role of atmospheric chem-
 1054 istry in the climate impacts of stratospheric volcanic injections, *Nature Geo-*
 1055 *science*, doi:10.1038/ngeo2771.
- 1056 Mastin, L. (2014), Testing the accuracy of a 1-D volcanic plume model in estimat-
 1057 ing mass eruption rate, *Journal of Geophysical Research: Atmospheres*, 119(5),
 1058 2474–2495, doi:10.1002/2013JD020604.
- 1059 Mastin, L., M. Guffanti, R. Servranckx, P. Webley, S. Barsotti, K. Dean, A. Durant,
 1060 J. Ewert, A. Neri, W. Rose, et al. (2009), A multidisciplinary effort to assign re-
 1061 alistic source parameters to models of volcanic ash-cloud transport and dispersion
 1062 during eruptions, *Journal of Volcanology and Geothermal Research*, 186(1), 10–21,
 1063 doi:10.1016/j.jvolgeores.2009.01.008.
- 1064 Mastrandrea, M. D., C. B. Field, T. F. Stocker, O. Edenhofer, K. L. Ebi, D. J.
 1065 Frame, H. Held, E. Kriegler, K. J. Mach, P. R. Matschoss, et al. (2010), Guidance
 1066 note for lead authors of the IPCC fifth assessment report on consistent treatment
 1067 of uncertainties.
- 1068 McCoy, D. T., and D. L. Hartmann (2015), Observations of a substantial cloud-
 1069 aerosol indirect effect during the 2014–2015 Bárðarbunga-Veiðivötn fissure
 1070 eruption in Iceland, *Geophysical Research Letters*, 42(23), 10,409–10,414, doi:
 1071 10.1002/2015GL067070.
- 1072 McGregor, S., and A. Timmermann (2010), The effect of explosive tropical volcan-
 1073 ism on ENSO, *Journal of Climate*, 24, 2178–2191, doi:10.1175/2010JCLI3990.1.
- 1074 McGuire, W. J., R. J. Howarth, C. R. Firth, A. R. Solow, A. D. Pullen, S. J. Saun-
 1075 ders, I. S. Stewart, and C. Vita-Finzi (1997), Correlation between rate of sea-

- 1076 level change and frequency of explosive volcanism in the mediterranean, *Nature*,
 1077 389(6650), 473–476, doi:10.1038/38998.
- 1078 McLandress, C., and T. G. Shepherd (2009), Simulated anthropogenic changes in
 1079 the Brewer-Dobson circulation, including its extension to high latitudes, *Journal*
 1080 *of Climate*, 22(6), 1516–1540, doi:10.1175/2008JCLI2679.1.
- 1081 Mignot, J., M. Khodri, C. Frankignoul, and J. Servonnat (2011), Volcanic impact on
 1082 the Atlantic ocean over the last millennium, *Climate of the Past*, 7(4), 1439–1455,
 1083 doi:10.5194/cp-7-1439-2011.
- 1084 Mills, M. J., A. Schmidt, R. Easter, S. Solomon, D. E. Kinnison, S. J. Ghan,
 1085 R. R. Neely, D. R. Marsh, A. Conley, C. G. Bardeen, et al. (2016), Global
 1086 volcanic aerosol properties derived from emissions, 1990–2014, using CESM1
 1087 (WACCM), *Journal of Geophysical Research: Atmospheres*, 121(5), 2332–2348,
 1088 doi:10.1002/2015JD024290.
- 1089 Mitchell, D., P. Thorne, P. Stott, and L. Gray (2013), Revisiting the controversial
 1090 issue of tropical tropospheric temperature trends, *Geophysical Research Letters*,
 1091 40(11), 2801–2806, doi:10.1002/grl.50465.
- 1092 Morton, B. (1957), Buoyant plumes in a moist atmosphere, *Journal of Fluid Me-*
 1093 *chanics*, 2(02), 127–144, doi:10.1017/S0022112057000038.
- 1094 Morton, B. R., G. Taylor, and J. S. Turner (1956), Turbulent gravitational convec-
 1095 tion from maintained and instantaneous sources, *Proceedings of the Royal Society*
 1096 *of London A: Mathematical, Physical and Engineering Sciences*, 234(1196), 1–23,
 1097 doi:10.1098/rspa.1956.0011.
- 1098 Newhall, C. G., and S. Self (1982), The Volcanic Explosivity Index (VEI): an es-
 1099 timate of explosive magnitude for historical volcanism, *Journal of Geophysical*
 1100 *Research*, 87, 1231–1238, doi:10.1029/JC087iC02p01231.
- 1101 Oppenheimer, C. (2003), Climatic, environmental and human consequences of the
 1102 largest known historic eruption: Tambora volcano (Indonesia) 1815, *Progress in*
 1103 *physical geography*, 27(2), 230–259, doi:10.1191/0309133303pp379ra.
- 1104 Prata, A., S. Carn, A. Stohl, and J. Kerkmann (2007), Long range transport and
 1105 fate of a stratospheric volcanic cloud from Soufrière Hills volcano, Montserrat, *At-*
 1106 *mospheric Chemistry and Physics*, 7(19), 5093–5103, doi:10.5194/acp-7-5093-2007.
- 1107 Radić, V., A. J. Cannon, B. Menounos, and N. Gi (2015), Future changes in autumn
 1108 atmospheric river events in British Columbia, Canada, as projected by CMIP5

- 1109 global climate models, *Journal of Geophysical Research: Atmospheres*, *120*(18),
 1110 9279–9302, doi:10.1002/2015JD023279.
- 1111 Ridley, D. A., S. Solomon, J. E. Barnes, V. D. Burlakov, T. Deshler, S. I. Dolgii,
 1112 A. B. Herber, T. Nagai, R. R. Neely, A. V. Nevzorov, C. Ritter, T. Sakai, B. D.
 1113 Santer, M. Sato, A. Schmidt, O. Uchino, and J. P. Vernier (2014), Total volcanic
 1114 stratospheric aerosol optical depths and implications for global climate change,
 1115 *Geophysical Research Letters*, *41*(22), 7763–7769, doi:10.1002/2014GL061541.
- 1116 Rieger, L. A., A. E. Bourassa, and D. A. Degenstein (2015), Merging the OSIRIS
 1117 and SAGE II stratospheric aerosol records, *Journal of Geophysical Research: At-*
 1118 *mospheres*, *120*(17), 8890–8904, doi:10.1002/2015JD023133.
- 1119 Robock, A. (2000), Volcanic eruptions and climate, *Reviews of Geophysics*, *38*, 191–
 1120 219, doi:10.1029/1998RG000054.
- 1121 Rymer, H. (2015), *The Encyclopedia of Volcanoes (Second Edition)*, pp. 895 – 896,
 1122 Academic press, doi:10.1016/B978-0-12-385938-9.02009-5.
- 1123 Sanford, T., P. C. Frumhoff, A. Luers, and J. Gullledge (2014), The climate policy
 1124 narrative for a dangerously warming world, *Nature Climate Change*, *4*(3), 164–
 1125 166, doi:10.1038/nclimate2148.
- 1126 Santer, B., C. Bonfils, J. Painter, M. Zelinka, C. Mears, S. Solomon, G. Schmidt,
 1127 J. Fyfe, J. Cole, L. Nazarenko, K. Taylor, and F. Wentz (2014), Volcanic contri-
 1128 bution to decadal changes in tropospheric temperature, *Nature Geoscience*, *7*,
 1129 185–189, doi:10.1038/ngeo2098.
- 1130 Santer, B. D., M. F. Wehner, T. Wigley, R. Sausen, G. Meehl, K. Taylor, C. Am-
 1131 mann, J. Arblaster, W. Washington, J. Boyle, et al. (2003), Contributions of
 1132 anthropogenic and natural forcing to recent tropopause height changes, *Science*,
 1133 *301*(5632), 479–483, doi:10.1126/science.1084123.
- 1134 Santer, B. D., S. Solomon, C. Bonfils, M. D. Zelinka, J. F. Painter, F. Beltran, J. C.
 1135 Fyfe, G. Johannesson, C. Mears, D. A. Ridley, J.-P. Vernier, and F. J. Wentz
 1136 (2015), Observed multivariable signals of late 20th and early 21st century volcanic
 1137 activity, *Geophysical Research Letters*, *42*(2), 500–509, doi:10.1002/2014GL062366.
- 1138 Sato, M., J. E. Hansen, M. P. McCormick, and J. B. Pollack (1993), Stratospheric
 1139 aerosol optical depths, 1850–1990, *Journal of Geophysical Research: Atmospheres*,
 1140 *98*(D12), 22,987–22,994, doi:10.1029/93JD02553.

- 1141 Schmidt, A., K. S. Carslaw, G. W. Mann, A. Rap, K. J. Pringle, D. V. Spracklen,
 1142 M. Wilson, and P. M. Forster (2012), Importance of tropospheric volcanic aerosol
 1143 for indirect radiative forcing of climate, *Atmospheric Chemistry and Physics*,
 1144 *12*(16), 7321–7339, doi:10.5194/acp-12-7321-2012.
- 1145 Schmidt, A., S. Leadbetter, N. Theys, E. Carboni, C. S. Witham, J. A. Stevenson,
 1146 C. E. Birch, T. Thordarson, S. Turnock, S. Barsotti, et al. (2015), Satellite detec-
 1147 tion, long-range transport, and air quality impacts of volcanic sulfur dioxide from
 1148 the 2014–2015 flood lava eruption at Bárðarbunga (Iceland), *Journal of Geophysi-
 1149 cal Research: Atmospheres*, *120*(18), 9739–9757, doi:10.1002/2015JD023638.
- 1150 Schmidt, A., R. A. Skeffington, T. Thordarson, S. Self, P. M. Forster, A. Rap,
 1151 A. Ridgwell, D. Fowler, M. Wilson, G. W. Mann, et al. (2016), Selective environ-
 1152 mental stress from sulphur emitted by continental flood basalt eruptions, *Nature
 1153 Geoscience*, *9*, 77–82, doi:10.1038/ngeo2588.
- 1154 Sherwood, S. C., and N. Nishant (2015), Atmospheric changes through 2012
 1155 as shown by iteratively homogenized radiosonde temperature and wind data
 1156 (IUKv2), *Environmental Research Letters*, *10*(5), 054,007, doi:10.1088/1748-
 1157 9326/10/5/054007.
- 1158 Shindell, D. T., G. A. Schmidt, M. E. Mann, and G. Faluvegi (2004), Dynamic win-
 1159 ter climate response to large tropical volcanic eruptions since 1600, *Journal of
 1160 Geophysical Research: Atmospheres*, *109*(D5), doi:10.1029/2003JD004151.
- 1161 Simmons, A., P. Poli, D. Dee, P. Berrisford, H. Hersbach, S. Kobayashi, and
 1162 C. Peubey (2014), Estimating low-frequency variability and trends in atmospheric
 1163 temperature using ERA-Interim, *Quarterly Journal of the Royal Meteorological
 1164 Society*, *140*(679), 329–353, doi:10.1002/qj.2317.
- 1165 Solomon, S., J. S. Daniel, R. R. Neely, J.-P. Vernier, E. G. Dutton, and L. W.
 1166 Thomason (2011), The persistently variable "background" stratospheric
 1167 aerosol layer and global climate change, *Science*, *333*(6044), 866–870, doi:
 1168 10.1126/science.1206027.
- 1169 Stenchikov, G. L., K. Hamilton, R. J. Stouffer, A. Robock, V. Ramaswamy, B. San-
 1170 ter, and H.-F. Graf (2006), Arctic Oscillation response to volcanic eruptions in
 1171 the IPCC AR4 climate models, *Journal of Geophysical Research*, *111*(D7), doi:
 1172 10.1029/2005JD006286.

- 1173 Stoffel, M., M. Khodri, C. Corona, S. Guillet, V. Poulain, S. Bekki, J. Guiot, B. H.
 1174 Luckman, C. Oppenheimer, N. Lebas, M. Beniston, and V. Masson-Delmotte
 1175 (2015), Estimates of volcanic-induced cooling in the northern hemisphere over the
 1176 past 1,500 years, *Nature Geoscience*, *8*, 784–788, doi:10.1038/ngeo2526.
- 1177 Tabazadeh, A., and R. Turco (1993), Stratospheric chlorine injection by volcanic
 1178 eruptions: HCl scavenging and implications for ozone, *Science*, *260*(5111), 1082–
 1179 1086, doi:10.1126/science.260.5111.1082.
- 1180 Taylor, K. E., R. J. Stouffer, and G. A. Meehl (2012), An overview of CMIP5 and
 1181 the experiment design, *Bulletin of the American Meteorological Society*, *93*(4),
 1182 485–498, doi:10.1175/bams-d-11-00094.1.
- 1183 Textor, C., H.-F. Graf, M. Herzog, and J. Oberhuber (2003), Injection of gases into
 1184 the stratosphere by explosive volcanic eruptions, *Journal of Geophysical Research:
 1185 Atmospheres*, *108*(D19), doi:10.1029/2002jd002987.
- 1186 Thordarson, T., and S. Self (2003), Atmospheric and environmental effects of the
 1187 1783–1784 Laki eruption: A review and reassessment, *Journal of Geophysical Re-
 1188 search: Atmospheres*, *108*(D1), AAC 7–1–AAC 7–29, doi:10.1029/2001JD002042,
 1189 4011.
- 1190 Timmreck, C. (2012), Modeling the climatic effects of large explosive volcanic
 1191 eruptions, *Wiley Interdisciplinary Reviews: Climate Change*, *3*(6), 545–564, doi:
 1192 10.1002/wcc.192.
- 1193 Toohey, M., K. Krüger, U. Niemeier, and C. Timmreck (2011), The influence of
 1194 eruption season on the global aerosol evolution and radiative impact of tropical
 1195 volcanic eruptions, *Atmospheric Chemistry and Physics*, *11*(23), 12,351–12,367,
 1196 doi:10.5194/acp-11-12351-2011.
- 1197 Toohey, M., K. Krüger, M. Sigl, F. Stordal, and H. Svensen (2016a), Climatic and
 1198 societal impacts of a volcanic double event at the dawn of the Middle Ages, *Cli-
 1199 matic Change*, *136*(3), 401–412, doi:10.1007/s10584-016-1648-7.
- 1200 Toohey, M., B. Stevens, H. Schmidt, and C. Timmreck (2016b), Easy Volcanic
 1201 Aerosol (EVA v1.0): An idealized forcing generator for climate simulations, *Geo-
 1202 scientific Model Development Discussions*, *2016*, 1–40, doi:10.5194/gmd-2016-83.
- 1203 Tupper, A., I. Itikarai, M. Richards, F. Prata, S. Carn, and D. Rosenfeld (2007),
 1204 Facing the challenges of the international airways volcano watch: The 2004/05
 1205 eruptions of Manam, Papua New Guinea, *Weather and Forecasting*, *22*(1), 175–

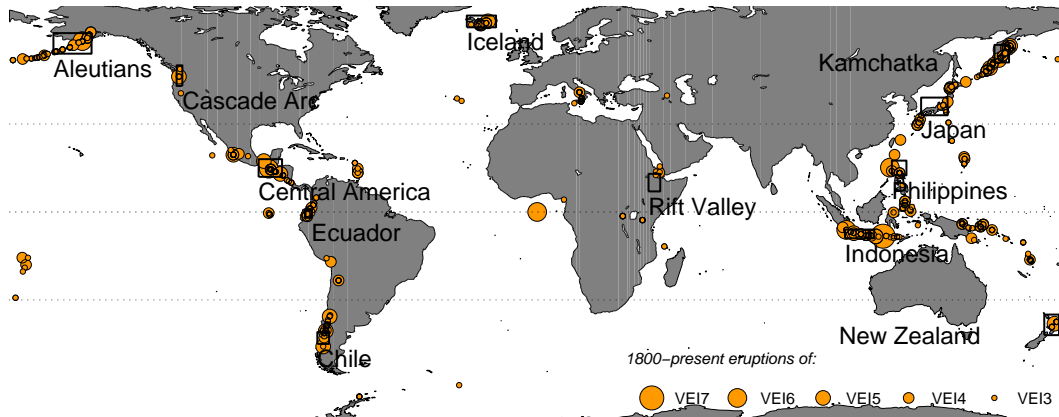
- 1206 191, doi:10.1175/waf974.1.
- 1207 Uppala, S. M., P. Kållberg, A. Simmons, U. Andrae, V. Bechtold, M. Fiorino,
 1208 J. Gibson, J. Haseler, A. Hernandez, G. Kelly, et al. (2005), The ERA-40 re-
 1209 analysis, *Quarterly Journal of the Royal Meteorological Society*, *131*(612), 2961–
 1210 3012, doi:10.1256/qj.04.176.
- 1211 Van Vuuren, D., J. Edmonds, M. Kainuma, K. Riahi, A. Thomson, K. Hibbard,
 1212 G. Hurtt, T. Kram, V. Krey, J.-F. Lamarque, T. Masui, M. Meinshausen, N. Na-
 1213 kicenovic, S. Smith, and S. Rose (2011), The representative concentration path-
 1214 ways: an overview, *Climatic Change*, *109*(1-2), 5–31, doi:10.1007/s10584-011-0148-
 1215 z.
- 1216 Vernier, J.-P., L. W. Thomason, T. D. Fairlie, P. Minnis, R. Palikonda, and
 1217 K. M. Bedka (2013), Comment on "Large volcanic aerosol load in the strato-
 1218 sphere linked to asian monsoon transport", *Science*, *339*(6120), 647–647, doi:
 1219 10.1126/science.1227817.
- 1220 Waythomas, C. F., W. E. Scott, S. G. Prejean, D. J. Schneider, P. Izbekov, and
 1221 C. J. Nye (2010), The 7–8 August 2008 eruption of Kasatochi volcano, central
 1222 Aleutian Islands, Alaska, *Journal of Geophysical Research: Solid Earth*, *115*(B12),
 1223 doi:10.1029/2010JB007437.
- 1224 Wilson, L., R. Sparks, T. Huang, and N. Watkins (1978), The control of volcanic
 1225 column heights by eruption energetics and dynamics, *Journal of Geophysical Re-
 1226 search: Solid Earth*, *83*(B4), 1829–1836, doi:10.1029/JB083iB04p01829.
- 1227 Woodhouse, M., A. Hogg, J. Phillips, and R. S. J. Sparks (2013), Interaction be-
 1228 tween volcanic plumes and wind during the 2010 Eyjafjallajökull eruption, Ice-
 1229 land, *Journal of Geophysical Research*, *118*(1), 92–109, doi:10.1029/2012JB009592.
- 1230 Woodhouse, M. J., A. J. Hogg, J. C. Phillips, and J. C. Rougier (2015), Uncer-
 1231 tainty analysis of a model of wind-blown volcanic plumes, *Bulletin of Volcanology*,
 1232 *77*(10), 1–28, doi:10.1007/s00445-015-0959-2.
- 1233 Woods, A. (1988), The fluid dynamics and thermodynamics of eruption columns,
 1234 *Bulletin of Volcanology*, *50*(3), 169–193, doi:10.1007/BF01079681.
- 1235 Woods, A. (1993), Moist convection and the injection of volcanic ash into the at-
 1236 mosphere, *Journal of Geophysical Research: Solid Earth*, *98*(B10), 17,627–17,636,
 1237 doi:10.1029/93JB00718.

- 1238 Woods, A. (2010), Turbulent plumes in nature, *Annual Review of Fluid Mechanics*,
1239 42, 391–412, doi:10.1146/annurev-fluid-121108-145430.
- 1240 Woods, A., and K. Wohletz (1991), Dimensions and dynamics of co-ignimbrite erup-
1241 tion columns, *Nature*, 350(6315), 225–227, doi:10.1038/350225a0.
- 1242 Wu, T., L. Song, W. Li, Z. Wang, H. Zhang, X. Xin, Y. Zhang, L. Zhang, J. Li,
1243 F. Wu, Y. Liu, F. Zhang, X. Shi, M. Chu, J. Zhang, Y. Fang, F. Wang, Y. Lu,
1244 X. Liu, M. Wei, Q. Liu, W. Zhou, M. Dong, Q. Zhao, J. Ji, L. Li, and M. Zhou
1245 (2014), An overview of BCC climate system model development and application
1246 for climate change studies, *Journal of Meteorological Research*, 28(1), 34–56, doi:
1247 10.1007/s13351-014-3041-7.
- 1248 Zanchettin, D., M. Khodri, C. Timmreck, M. Toohey, A. Schmidt, E. P. Gerber,
1249 G. Hegerl, A. Robock, F. S. Pausata, W. T. Ball, S. E. Bauer, S. Bekki, S. S.
1250 Dhomse, A. N. LeGrande, G. W. Mann, L. Marshall, M. Mills, M. Marchand,
1251 U. Niemeier, V. Paulain, A. Rubino, A. Stenke, K. Tsigaridis, and F. Tummon
1252 (2016), The Model Intercomparison Project on the climatic response to Volcanic
1253 forcing (VolMIP): Experimental design and forcing input data, *Geoscientific*
1254 *Model Development Discussions*, 2016, 1–33, doi:10.5194/gmd-2016-68.

1255 **Table 1.** Values of parameters used in the integral volcanic plume model (greek symbols) and
 1256 of eruption source conditions (symbols with 0-subscript).

| Parameter | Symbol | Unit | Value | Range |
|--------------------------------|-----------|-------------------|----------|-------------------------------|
| Radial entrainment coefficient | α | - | 0.1 | 0.07 – 0.13 |
| Wind entrainment coefficient | β | - | 0.7 | 0.35 – 1 |
| Condensation rate | λ | s^{-1} | 0 | 0 – 0.098 |
| Temperature | T_0 | K | 1200 | 1000 – 1400 |
| Gas mass fraction | n_0 | - | 0.04 | 0.01 – 0.07 |
| Velocity | U_0 | m s^{-1} | 75 – 300 | 75 – 300 |
| Vent radius | R_0 | m | 10 – 150 | 10 – 150 |
| Vent height | H_0 | m | 1500 | local topography ^a |

^aVent height is sampled from a distribution representative of the altitude of volcanoes in the region considered (cf. Supporting Information S4) or from the *Carn et al.* [2016] dataset



1274 **Figure 1.** Global map with the 12 volcanically active regions selected for this study (black
 1275 rectangles). Orange dots show large explosive eruptions (VEI of 3 to 7) for the last 2 centuries
 1276 (from Global Volcanism Program database).

1257 **Table 2.** Subset of the volcanic eruptions chosen to test the impact of climate change on plume
 1258 height. The top group consists of eruptions with relatively large stratospheric injections in the
 1259 late 20th century. The middle group consists of eruptions with relatively small stratospheric in-
 1260 jections in the early 21st century with a distinct footprint on climate [*Santer et al.*, 2015]. The
 1261 bottom group consists of basaltic eruptions, either stratospheric or tropospheric. SO₂ mass and
 1262 plume altitudes are taken from *Carn et al.* [2016], except for the Laki eruptions [*Thordarson and*
 1263 *Self*, 2003], and the range indicated for plume altitude corresponds to estimated range from other
 1264 studies, when available. We also indicate the stratospheric aerosol optical depth peak after the
 1265 eruption, defined as the stratospheric aerosol optical depth of the month preceding the eruption
 1266 subtracted from the first peak in the global monthly mean stratospheric aerosol optical depth in
 1267 the 12 months following an eruption.

| Volcano | Date | Country | Latitude | Vent Altitude (km) | SO ₂ Plume Altitude (km) | Estimated M ₀ (kg s ⁻¹) | SO ₂ (Mt) | Δτ |
|-----------------|--------------------------|------------------|----------|--------------------|--|--|----------------------|------------------------|
| El Chichón, A | Mar.29, 1982 | Mexico | 17.4°N | 1.2 | 17 ^a | 1.3 10 ⁷ | 0.75 ^a | 9.2 10 ^{-2 b} |
| El Chichón, B | Apr.4, 1982 | Mexico | 17.4°N | 1.2 | 28 ^a | 3.0 10 ⁸ | 7 ^a | 9.2 10 ^{-2 b} |
| Mt Pinatubo | Jun.15, 1991 | Philippines | 15.0°N | 1.7 | 25 ^a (17-28) ^{c,d,e} | 1.7 10 ⁸ | 18 ^a | 1.4 10 ^{-1 b} |
| Manam | Jan.27, 2005 | Papua New Guinea | 4.1°S | 1.8 | 24 ^a (18-24) ^{c,d,f} | 8.1 10 ⁷ | 0.14 ^a | 8.0 10 ^{-4 b} |
| Soufrière Hills | May 20, 2006 | Montserrat (UK) | 16.7°N | 0.2 | 20 ^a (17-21) ^{c,d,g} | 4.1 10 ⁷ | 0.2 ^a | 2.2 10 ^{-3 b} |
| Kasatochi | Aug.7, 2008 | Russia | 52.2°N | 0.3 | 15 ^a (10-18) ^{c,d,h} | 3.4 10 ⁷ | 2 ^a | 1.5 10 ^{-3 b} |
| Sarychev | Jun.16, 2009 | Russia | 48.1°N | 1.5 | 17 ^a (11-17) ^{c,d} | 3.8 10 ⁷ | 1.2 ^a | 2.6 10 ^{-3 b} |
| Merapi | Nov.4, 2010 | Indonesia | 7.5°S | 3 | 17 ^a (14-18) ^{c,d} | 5.5 10 ⁶ | 0.3 ^a | 1.0 10 ^{-3 b} |
| Nabro | Jun.13, 2011 | Eritrea | 13.4°N | 2.2 | 18 ^a (10-19) ^{c,d,i,j,k,l} | 1.8 10 ⁷ | 0.68 ^a | 3.4 10 ^{-3 b} |
| Kelut | Feb.13, 2014 | Indonesia | 8.0°S | 1.7 | 19 ^a (17-26) ^d | 2.9 10 ⁷ | 0.2 ^a | 2.5 10 ^{-3 k} |
| Laki | Jun.8, 1783 - Feb.7 1784 | Iceland | 64°N | 1.7 | 11 (9-13) ⁿ | 3.7 10 ⁶ | 122 ⁿ | - |
| Etna | Aug.20, 2011 | Italy | 37.7°N | 3.4 | 9 ^a | 5.6 10 ⁵ | 0.004 ^a | - |
| Bárðarbunga | Sep. 2014 - Dec. 2014 | Iceland | 64.6°N | 2 | 5 ^a (3-5) ^o | 7.1 10 ⁴ | 4.3 ^a | - |

^a *Carn et al.* [2016], ^b *Sato et al.* [1993], ^c *Brühl et al.* [2015], ^d *Mills et al.* [2016], ^e *Guo et al.* [2004], ^f *Tupper et al.* [2007], ^g *Prata et al.* [2007], ^h *Waythomas et al.* [2010],

ⁱ *Fromm et al.* [2013], ^j *Vernier et al.* [2013], ^k *Bourassa et al.* [2013], ^l *Clarisse et al.* [2014], ^m *Rieger et al.* [2015], ⁿ *Thordarson and Self* [2003], ^o *Schmidt et al.* [2015]

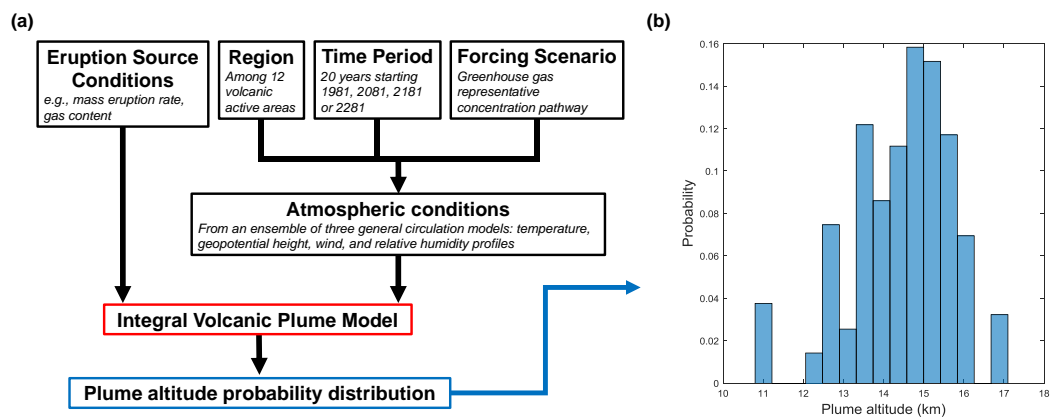
1268 **Table 3.** H^* reached for $M_0^*=1$, i.e., the median plume altitude, relative to the tropopause
 1269 height, reached for a mass eruption rate equal to the one required to reach the tropopause
 1270 in 1981-2000. The table provides the values for each region (rows), and period and scenario
 1271 (columns) considered in this study. Bold values indicate 99% significant changes relative to the
 1272 reference period (cf. Supporting Information S2 for details on the significance test).

| | 2081-2100 | | | 2181-2200 | | | 2281-2300 | | |
|-----------------|-------------|-------------|-------------|-------------|-------------|-------------|-------------|-------------|-------------|
| | RCP2.6 | RCP4.5 | RCP8.5 | RCP2.6 | RCP4.5 | RCP8.5 | RCP2.6 | RCP4.5 | RCP8.5 |
| Chile | 1 | 0.99 | 0.98 | 1 | 1 | 0.92 | 0.99 | 0.99 | 0.93 |
| New Zealand | 0.99 | 0.98 | 0.97 | 0.99 | 0.97 | 0.92 | 1.01 | 0.97 | 0.88 |
| Ecuador | 0.96 | 0.94 | 0.89 | 0.97 | 0.94 | 0.82 | 0.97 | 0.93 | 0.78 |
| Indonesia | 0.98 | 0.96 | 0.92 | 0.99 | 0.96 | 0.83 | 0.99 | 0.95 | 0.8 |
| Phillippines | 0.95 | 0.96 | 0.89 | 0.94 | 0.93 | 0.79 | 0.96 | 0.94 | 0.75 |
| Central America | 0.96 | 0.94 | 0.89 | 0.96 | 0.92 | 0.82 | 0.96 | 0.94 | 0.79 |
| African Ridge | 0.97 | 0.96 | 0.91 | 0.98 | 0.95 | 0.83 | 0.99 | 0.93 | 0.8 |
| Japan | 0.99 | 0.98 | 0.96 | 0.99 | 0.96 | 0.94 | 1 | 0.98 | 0.92 |
| Cascade | 1 | 0.99 | 0.96 | 0.99 | 0.98 | 0.93 | 1.02 | 0.99 | 0.92 |
| Kamchatka | 1.01 | 0.99 | 0.94 | 1.01 | 1 | 0.87 | 1.02 | 0.98 | 0.88 |
| Aleutians | 1 | 1 | 0.96 | 1.03 | 1.03 | 0.9 | 1.01 | 1 | 0.87 |
| Iceland | 1 | 0.99 | 0.94 | 0.99 | 0.99 | 0.9 | 1 | 0.98 | 0.88 |

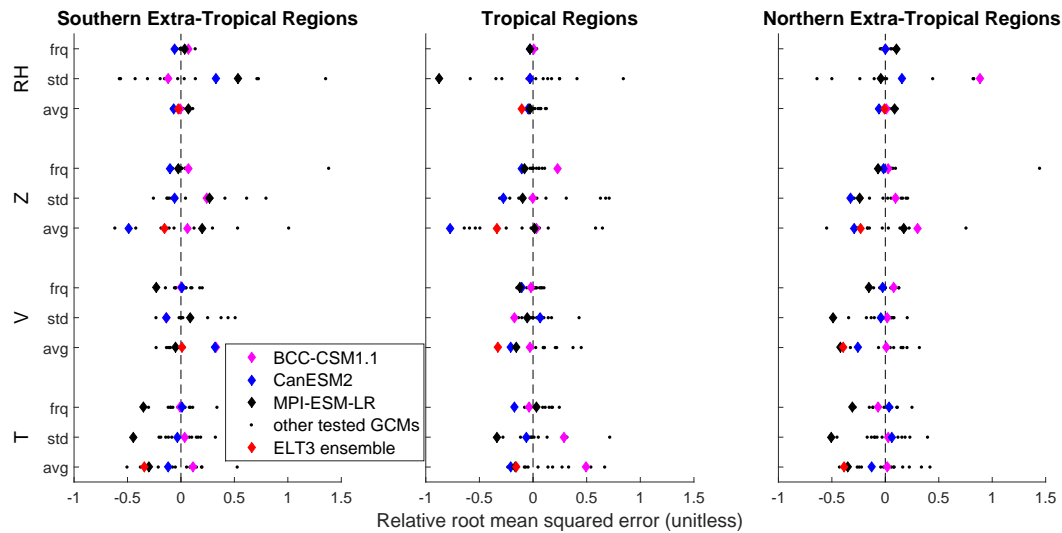
1273

Table 4. Same as Table 3, but showing the median M_0^* required to reach $H^*=1$.

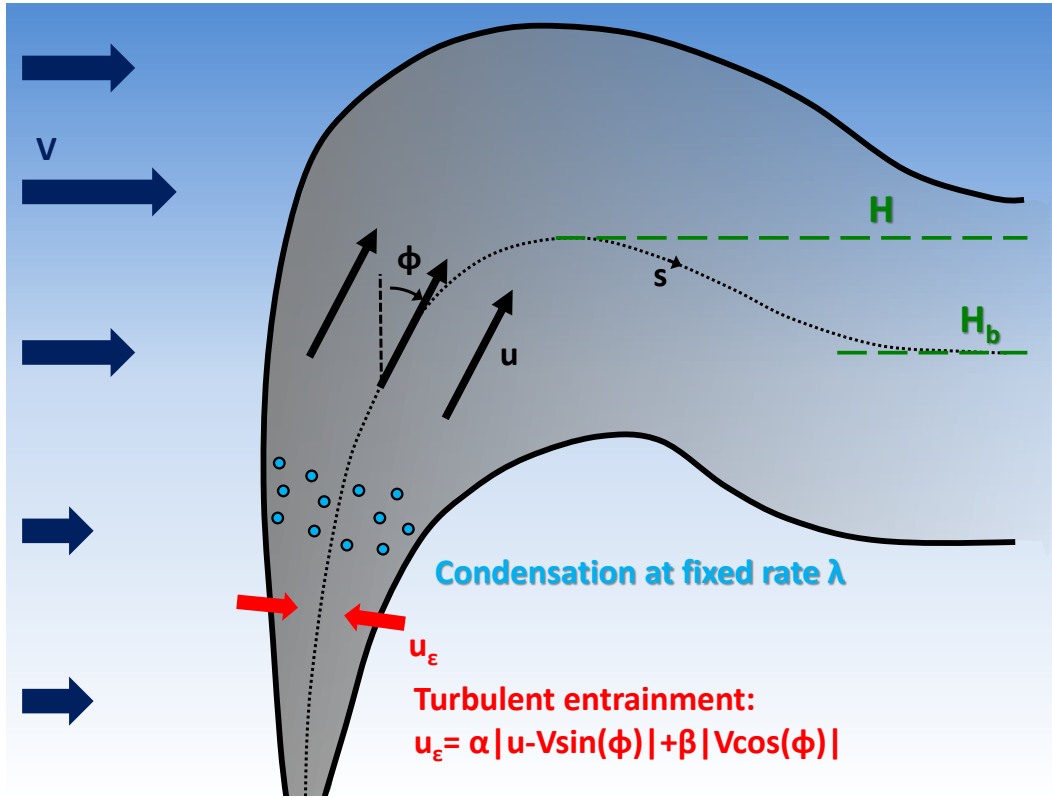
| | 2081-2100 | | | 2181-2200 | | | 2281-2300 | | |
|-----------------|-------------|-------------|-------------|-------------|-------------|-------------|-------------|-------------|-------------|
| | RCP2.6 | RCP4.5 | RCP8.5 | RCP2.6 | RCP4.5 | RCP8.5 | RCP2.6 | RCP4.5 | RCP8.5 |
| Chile | 0.98 | 1.04 | 1.1 | 0.99 | 1.01 | 1.53 | 1.05 | 1.08 | 1.42 |
| New Zealand | 1.09 | 1.15 | 1.18 | 1.03 | 1.19 | 1.57 | 0.95 | 1.19 | 1.85 |
| Ecuador | 1.24 | 1.32 | 1.66 | 1.14 | 1.33 | 2.13 | 1.17 | 1.37 | 2.46 |
| Indonesia | 1.12 | 1.23 | 1.5 | 1.09 | 1.24 | 2.11 | 1.06 | 1.29 | 2.52 |
| Phillippines | 1.32 | 1.25 | 1.65 | 1.34 | 1.39 | 2.29 | 1.21 | 1.3 | 2.8 |
| Central America | 1.24 | 1.38 | 1.79 | 1.25 | 1.52 | 2.41 | 1.21 | 1.37 | 2.75 |
| African Ridge | 1.14 | 1.21 | 1.59 | 1.11 | 1.27 | 2.27 | 1.08 | 1.41 | 2.44 |
| Japan | 1.04 | 1.1 | 1.23 | 1.04 | 1.2 | 1.25 | 0.98 | 1.11 | 1.42 |
| Cascade | 0.99 | 1.05 | 1.29 | 1.04 | 1.1 | 1.44 | 0.9 | 1.08 | 1.53 |
| Kamchatka | 0.95 | 1.06 | 1.36 | 0.93 | 0.99 | 1.86 | 0.88 | 1.09 | 1.92 |
| Aleutians | 1.01 | 1 | 1.2 | 0.86 | 0.87 | 1.69 | 0.97 | 1.02 | 1.84 |
| Iceland | 0.99 | 1.05 | 1.37 | 1.04 | 1.04 | 1.67 | 0.99 | 1.11 | 1.94 |



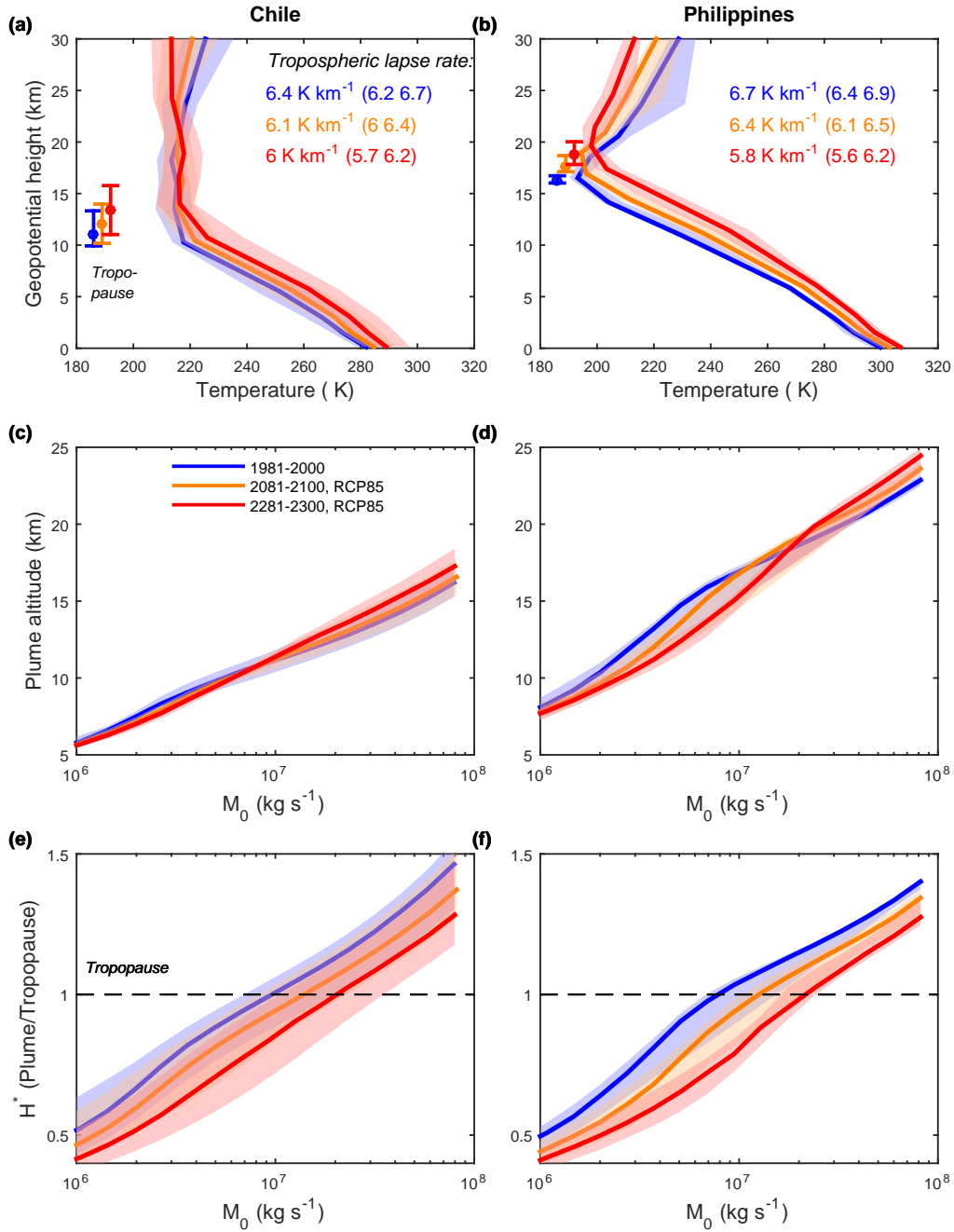
1277 **Figure 2.** (a) Flow chart summarizing the methodology used. To compute the plume altitude
 1278 probability distribution, we use an integral volcanic plume model. Eruption source conditions are
 1279 sampled from a fixed parameter space. Atmospheric conditions depends on the chosen region, pe-
 1280 riod, and greenhouse gas forcing (Representative Concentration Pathway). (b) Example of plume
 1281 altitude probability distribution obtained for $M_0=3.7 \cdot 10^6 \text{ kg s}^{-1}$ in the Philippines, for the 1981-
 1282 2000 period. The spread of the distribution is due to variability in temperature, geopotential
 1283 height and horizontal wind within the 20 year period.



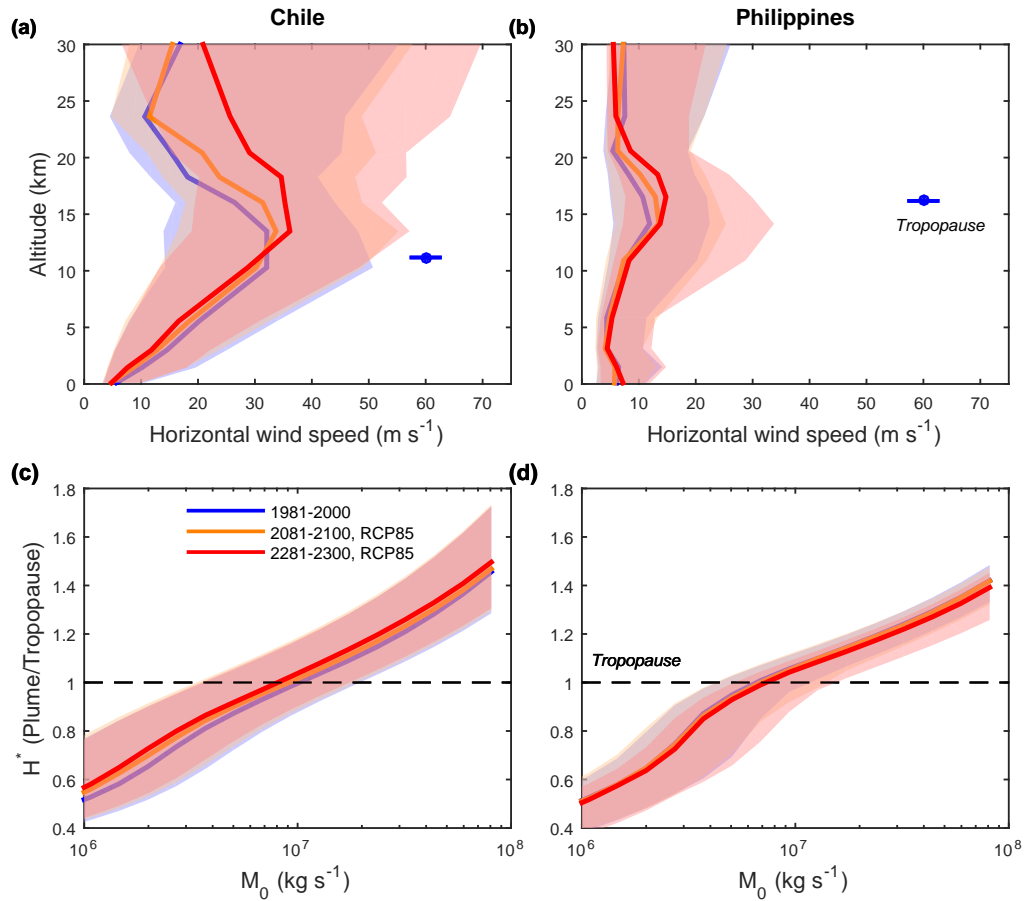
1284 **Figure 3.** Relative root mean square error (unitless, relative to the GCM median error) for
 1285 the T , V , Z , and RH fields, the three evaluation metrics (average, standard deviation and fre-
 1286 quency of characteristics patterns noted “avg”, “std” and “frq”, respectively on the figure) and
 1287 the three groups of regions. Small black dots show the relative error for the 16 GCMs tested
 1288 (Table S1). Diamonds symbols show the three GCMs selected to be used in this study (BCC-
 1289 CSM1.1, CanESM2 and MPI-ESM-LR) and their ensemble (ELT3) A negative error (left of the
 1290 dashed line) indicates that a GCM performs better than the median GCM. More details on the
 1291 GCM evaluation procedure are given in Supporting Information S1.



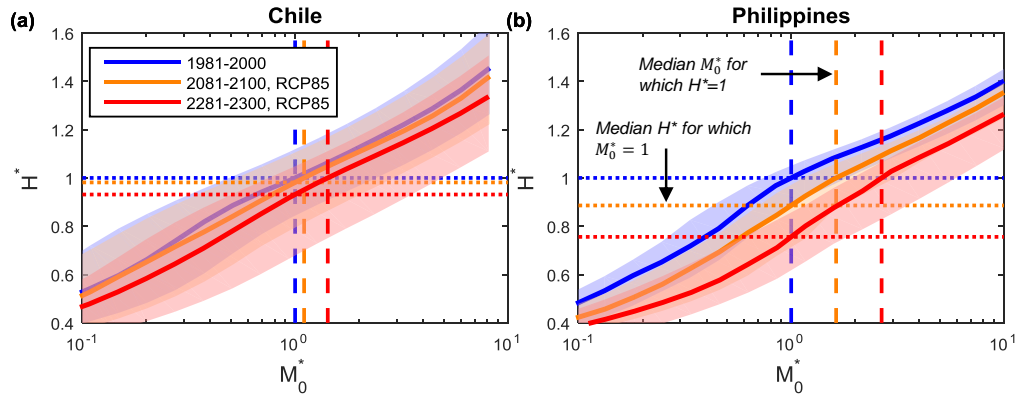
1292 **Figure 4.** Cartoon of a volcanic plume rising in the atmosphere and problem definition for
 1293 the integral volcanic plume model developed in Section 2.3. Plume properties, such as the plume
 1294 velocity u , depend only on the distance along the plume centerline s and plume properties pro-
 1295 files are top-hat (constant inside the plume and null outside). The inflow of atmospheric air into
 1296 the plume u_ϵ is proportional to the radial gradient of axial velocity between the plume and the
 1297 atmosphere ($|u - V \sin(\phi)|$) and to the radial gradient of ortho-axial velocity ($|V \cos(\phi)|$) where ϕ ,
 1298 the local plume deflection with respect to the vertical, defines the local axial direction. The green
 1299 dashed lines shows the maximum plume altitude H and the altitude of neutral buoyancy H_b .



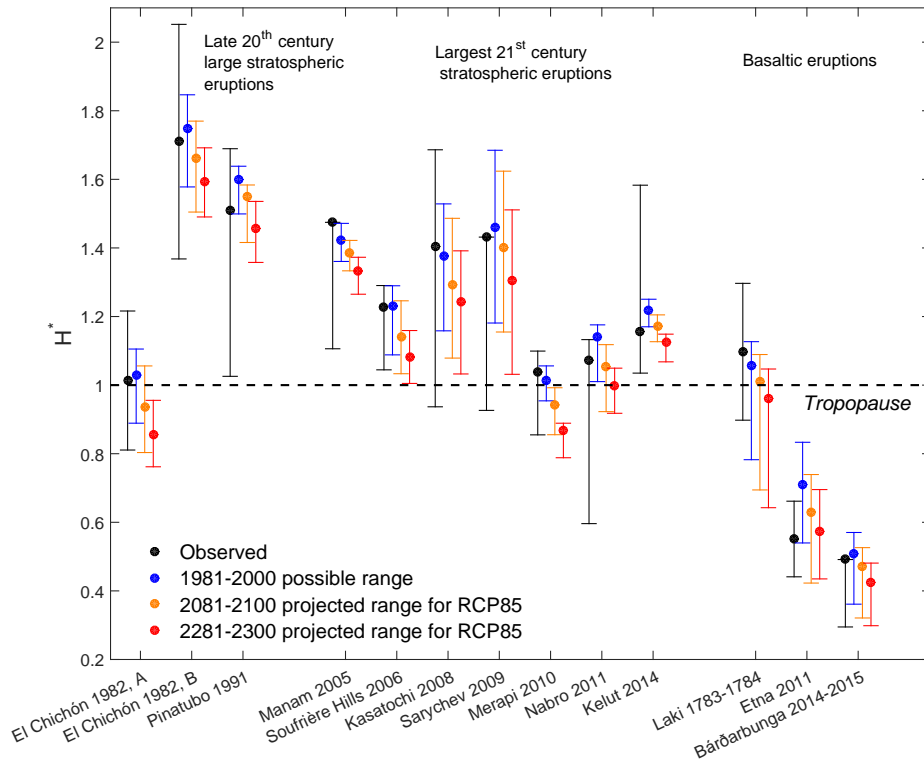
1300 **Figure 5.** Impacts of projected changes in temperature and geopotential height on volcanic
 1301 plume height for RCP8.5 (wind fixed to reference period average):
 1302 Left (a, c, e) and right (b, d, f) columns show results for the Chile and Philippines regions, re-
 1303 spectively. Top row (a, b) shows the temperature as a function of the geopotential height. Bold
 1304 lines show the median temperature, and shaded areas show the interval between the 5th and 95th
 1305 quantiles. The median tropopause height is shown by a square on the top row, with an error bar
 1306 showing the interval between the 5th and 95th quantiles. Blue, orange and red correspond to the
 1307 reference period (1981-2100), 2081-2100 RCP8.5, and 2281-2300 RCP8.5 projections, respectively.
 1308 The values of the median tropospheric lapse rate are indicated on panels (a) and (b) with 5th
 1309 and 95th quantiles indicated in parenthesis.
 1310 Center row (c, d) shows the maximum plume alti-
 1311 tude (H) as a function of the mass eruption rate. Bottom row (e, f) shows H^* , the ratio of the
 maximum plume height to tropopause height, as a function of the mass eruption rate.



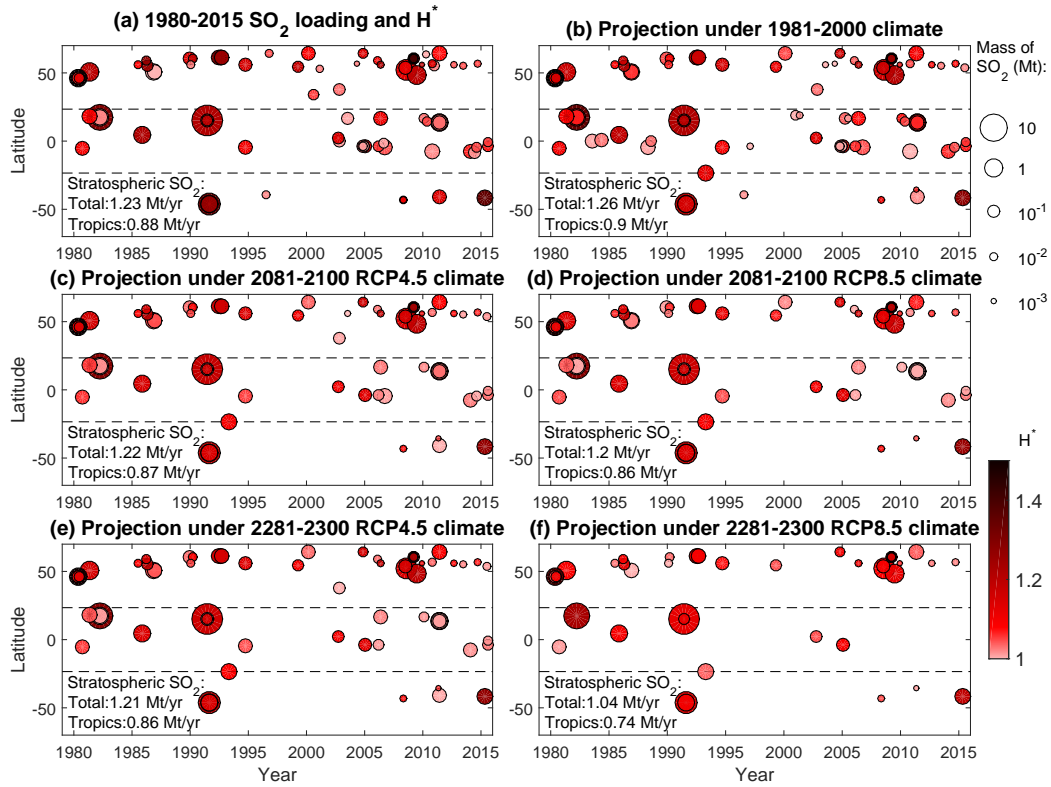
1312 **Figure 6.** Impact of projected changes in wind speed on volcanic plume height for RCP8.5
 1313 (temperature and geopotential height fixed to reference period average):
 1314 The temperature and geopotential height profiles are fixed to their averages for the reference
 1315 period. Top row (a, b) shows the horizontal wind speed as a function of the geopotential height.
 1316 Bottom row (c, d) shows H^* as a function of the mass eruption rate, with a fixed tropopause
 1317 altitude. Regions, color and shading are the same as for Figure 5.



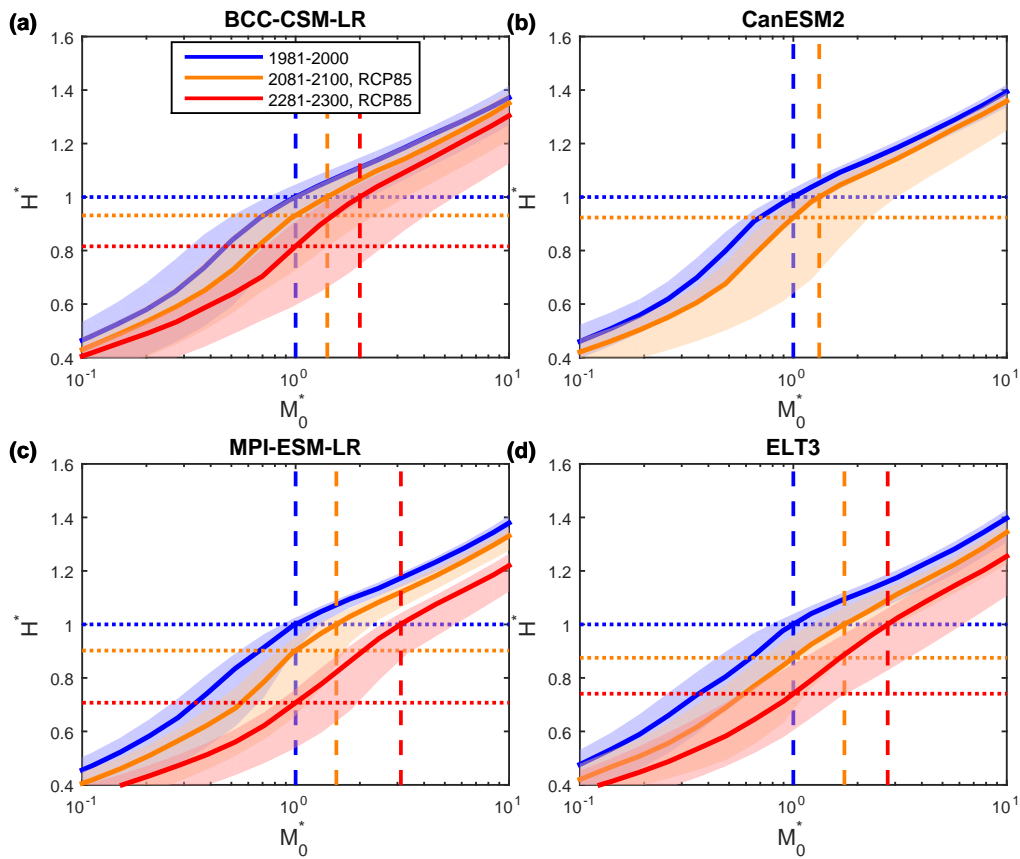
1318 **Figure 7.** Changes in H^* as a function of the dimensionless mass eruption rate M_0^* (nor-
 1319 malized to the median mass eruption rate required to reach the tropopause in 1981-2000) for
 1320 RCP8.5:
 1321 (a) and (b) show result for Chile and Philippines, respectively. Bold lines show the median, and
 1322 shadings show the interval between the 5th and 95th quantiles. Blue, orange and red correspond
 1323 to the reference period (1981-2100), 2081-2100 RCP8.5, and 2281-2300 RCP8.5 projections re-
 1324 spectively. Dotted lines of corresponding colors show the median value of H^* reached in $M_0^*=1$
 1325 (i.e., the median mass eruption rate for which the tropopause is reached in 1981-2000). Dashed
 1326 lines of corresponding colors show the median value of M_0^* required to reach $H^*=1$ (i.e., the
 1327 tropopause).



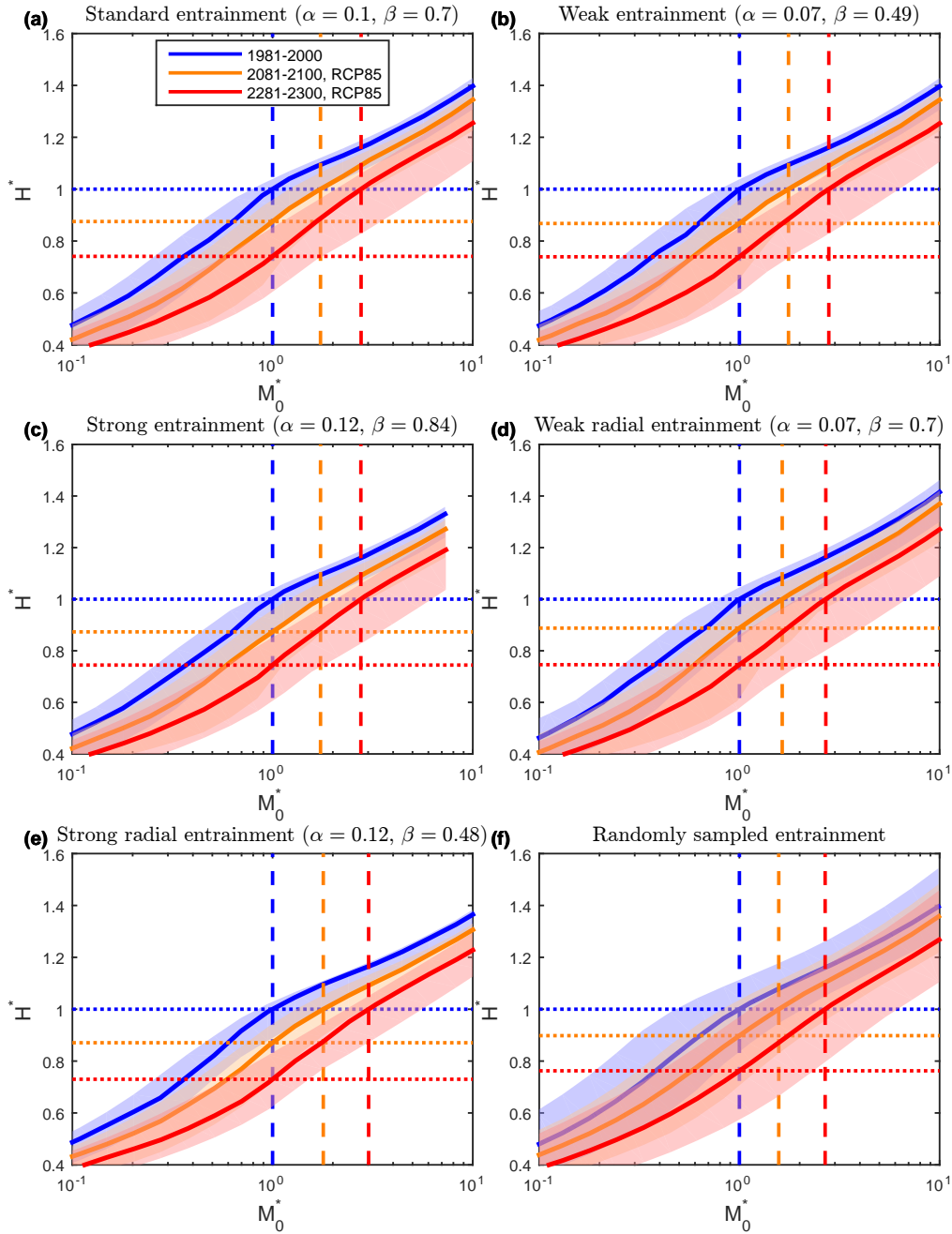
1328 **Figure 8.** Observed and projected H^* for past volcanic eruptions (Table 2):
 1329 Parameters for eruptions shown are listed in Table 2. The observed H^* , taken from *Carn et al.*
 1330 [2016], is shown in black, with vertical bars showing the estimated uncertainty based on height
 1331 estimates from different studies. We assume a relative uncertainty in plume height of $\pm 20\%$
 1332 where we could not find estimates different from *Carn et al.* [2016]. Blue, orange and red dots
 1333 show the predicted median H^* for the 1980-2000, 2081-2100 (RCP8.5) and 2281-2300 (RCP8.5)
 1334 periods, with vertical bars showing the 5th and 95th quantiles. The horizontal dashed line indi-
 1335 cates the tropopause, which corresponds to $H^*=1$.



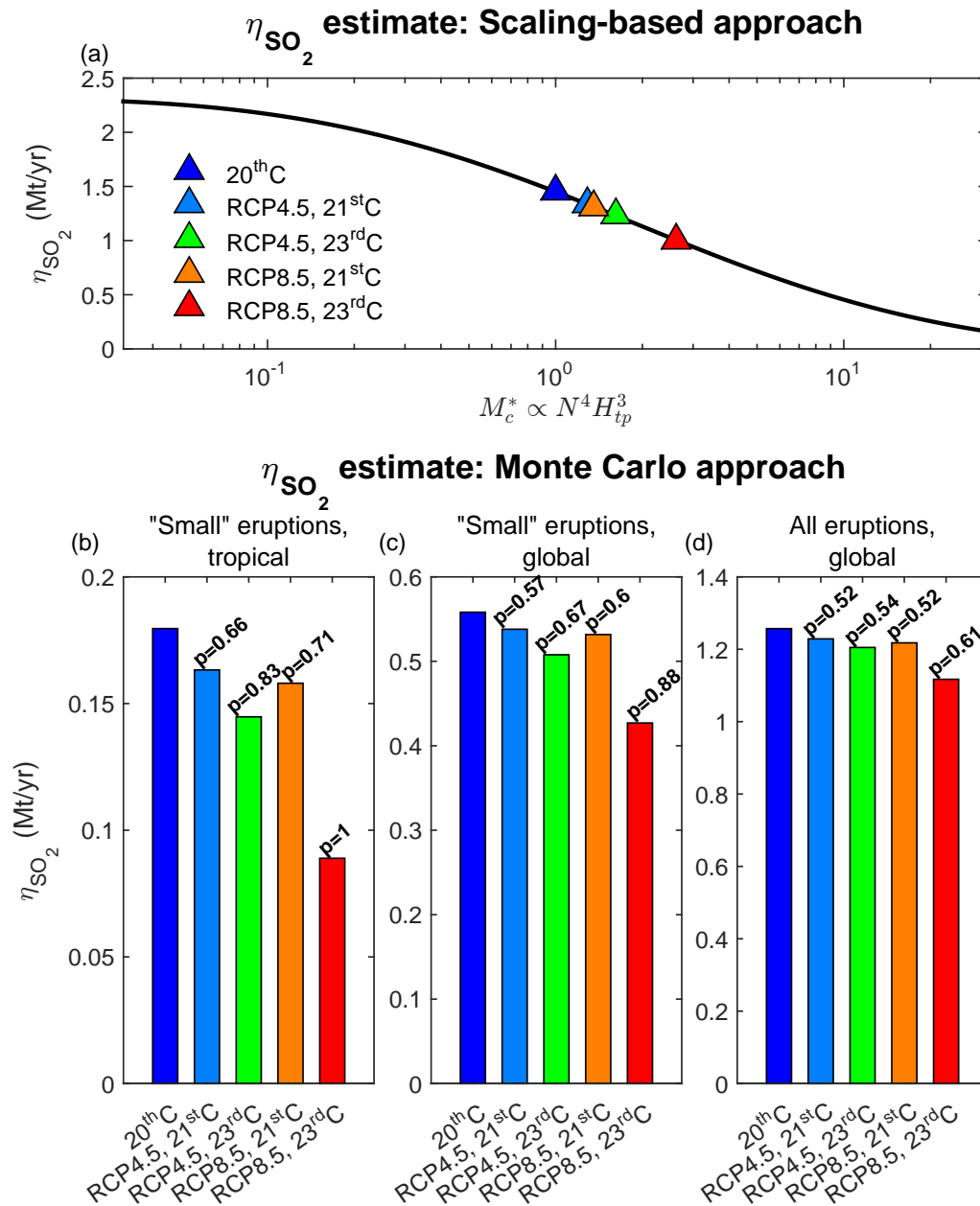
1336 **Figure 9.** Same as Figure 8, but showing observed and projected H^* (color scale) as a func-
 1337 tion of time and latitude for all eruptions retained in the *Carn et al.* [2016] dataset (dashed lines
 1338 show the tropics). The size of the circles is proportional to the logarithm of the mass of SO₂-
 1339 injected. Only stratospheric injections ($H^* \geq 1$) are shown. Panel (a) shows the original *Carn et al.*
 1340 [2016] dataset. In panels (b)-(f), we assume that the same sequence of eruptions occur (i.e., same
 1341 source parameters), but use climate conditions representative of the labeled period and RCP
 1342 scenario. For panels (b)-(f), we used the median H^* for each eruption. The total and tropical
 1343 volcanic flux of SO₂ into the stratosphere are indicated on each panel.



1344 **Figure 10.** Same as Figure 7, but with only the Philippines region shown. Panels (a), (b),
 1345 (c) and (d) show the result obtained when using projection from BCC-CSM-LR , CanESM2,
 1346 MPI-ESM-LR, and ELT3, respectively. Daily RCP runs for the 23rd century were not available
 1347 for CanESM2.



1348 **Figure 11.** Same as Figure 10, but showing sensitivity of the results to entrainment rates α
 1349 and β (Equation 4). Results are shown for the Philippines region using the ensemble ELT3. For
 1350 panel (a) to (e), we run the integral volcanic plume model with fixed values of α and β , labelled
 1351 in each panel. The ratio $\frac{\beta}{\alpha}$ is equal to 7, 10 and 4 for panels (a)-(c), panel (d) and panel (e), res-
 1352 pectively. For panel (f), we randomly sample values of α and β using a Monte-Carlo simulation;
 1353 we assume that α and $\frac{\beta}{\alpha}$ have normal distributions of mean 0.1 and 7 and width 0.015 and 1.5
 1354 respectively (based on a refined calibration of entrainment coefficients using the experiments of
 1355 *Carazzo et al. [2014]*).



1356 **Figure 12.** Projections of the volcanic SO_2 flux into the stratosphere η_{SO_2} , over a century, in
 1357 Mt/yr, for 1981-2000, 2081-2100 (RCP4.5 and RCP8.5) and 2281-2300 (RCP4.5 and RCP8.5).
 1358 Panel (a) shows η_{SO_2} as a function of the critical mass eruption rate M_c^* and the values of η_{SO_2}
 1359 for the different scenario estimated using the scaling-based approach of Section 4.3.1 (H_{tp} is the
 1360 tropopause height). Panels (b)-(d) show the median η_{SO_2} estimated using the Monte-Carlo ap-
 1361 proach of Section 4.3.2. Panel (b) shows the contribution of small (injecting less than 3 Mt of
 1362 SO_2) tropical eruptions, panel (c) the contribution of small eruptions, and panel (d) the total
 1363 flux. In panels (b)-(d), for future periods, the probability p for η_{SO_2} to be lower than under the
 1364 reference climate is indicated.